Biochimica et Biophysica Acta 1808 (2011) 2450–2465

Contents lists available at ScienceDirect

Biochimica et Biophysica Acta

journal homepage: www.elsevier.com/locate/bbamem

Molecular dynamics simulation of phase transitions in model lung surfactant monolayers

Susan L. Duncan, Indranil S. Dalal, Ronald G. Larson *

Dept. of Chemical Engineering, University of Michigan, 2300 Hayward St., 3074 H.H. Dow Building, Ann Arbor, MI 48109, USA

ARTICLE INFO

Article history:
Received 19 February 2011
Received in revised form 7 June 2011
Accepted 8 June 2011
Available online 13 July 2011

Keywords:
Pulmonary surfactant
Liquid condensed
Liquid expanded
Phase coexistence
Nucleation
Melting

ABSTRACT

To explore the role of individual lung surfactant components in liquid-condensed (LC)/liquid-expanded (LE) phase transitions the MARTINI coarse-grained (CG) model is used to simulate monolayers containing DPPC and additional lipid or peptide components. Our analysis suggests that the LC phase forms from the LE phase via a nucleation and growth mechanism, while the LC–LE transition occurs by melting that originates from defects in the monolayer. On the time scale of our simulations, DPPC monolayers display a substantial hysteresis between the ordering and disordering transitions, which is decreased by the addition of a second component. In binary mixtures of DPPC with lung surfactant peptide fragment SP-B_{1-25}, the ordered side of the hysteresis loop is abolished altogether, suggesting that SP-B_{1-25} effectively nucleates disorder in the monolayer on heating. SP-B_{1-25} is observed to perturb the packing of the surrounding lipids leading to local fluidization of the monolayer and to aggregate within the LE phase. In 1:1 DPPC:POPC monolayers, a high concentration of unsaturated phospholipid leads to a substantial decrease in the LC–LE and LE–LC transition temperatures. Adding cholesterol to pure DPPC increases the LC–LE and LE–LC transition temperatures and increases the order on the disordered side of the hysteresis loop leading to a phase of intermediate order, which could be the liquid-disordered (Ld) phase. Cholesterol is also observed to show a preference for LC–LE domain boundaries. The results of our molecular dynamics simulations coincide with many experimental observations and can help provide insight into the physiological roles of individual surfactant components.

1. Introduction

Lung surfactant (LS) is a mixture of phospholipids, fatty acids, neutral lipids, and surfactant proteins that forms the surface-active lining in the lungs and decreases the work of breathing by reducing and regulating the surface tension in the alveoli. Lung surfactant consists of approximately 90% lipids and 10% proteins by weight [1]. Of the surfactant lipids, about 80% are phosphatidylcholines, about half of which is dipalmitoylphosphatidylcholine (DPPC) [1]. Infants born prematurely lack functional lung surfactant and develop respiratory distress syndrome (RDS). Surfactant replacements have greatly reduced the mortality rate of RDS, but are not optimal [2]. Another form of RDS known as acute respiratory distress syndrome (ARDS) can develop in adults and has proven difficult to treat due to complications associated with underlying lung injury [3]. ARDS is often associated with the leakage of plasma proteins and other molecules into the lungs, resulting in inhibited lung surfactant function, which can be attributed to a variety of factors such as competitive adsorption. It is well known that in order to be effective, lung surfactant must display rapid adsorption, the ability to compress to near-zero surface tension upon end-expiration, and rapid respreading upon film expansion [4]. However, further research is needed to understand the mechanisms involved and the roles of individual surfactant components in the respiratory process, in order to aid the development of more efficient surfactant replacements to treat both neonatal and adult RDS.

The surfactant film undergoes rapid changes in surface area (and surface pressure) under the dynamic cycling occurring with each breath. Maintaining proper surfactant functionality under these demanding conditions requires a number of components. The primary component, dipalmitoylphosphatidylcholine (DPPC) has a high phase transition temperature of 41 °C [5], and therefore exists in the liquid condensed (LC) phase at body temperature. In the condensed phase DPPC is tightly packed and can be compressed to surface pressures well above the equilibrium spreading pressure (π_e) without collapse. For this reason DPPC is thought to be primarily responsible for the ability of lung surfactant to reach near-zero surface tension (high surface pressure). However, due to its rigidity at physiological temperature, DPPC exhibits poor respreadibility [6]. Additional surfactant components enhance the functionality of LS. Unsaturated phospholipids, such as palmitoyloleoylphosphatidylcholine (POPC), fluidize lung surfactant surface films increasing adsorption to the interface and are thought to enhance respreading [1]. Neutral lipids and fatty acids are also present, such as cholesterol (5–10 wt.% of

* Corresponding author. Tel.: +1 734 936 0772; fax: +1 734 763 0459.
E-mail address: rlarson@umich.edu (R.G. Larson).

0005-2736/$ – see front matter © 2011 Elsevier B.V. All rights reserved.
doi:10.1016/j.bbamem.2011.06.026

native surfactant), an important component of lung surfactant, which is systematically removed from most surfactant replacements [7]. Lung surfactant also contains surface-associated surfactant proteins SP-B and SP-C, which are essential to modulate the physical properties of the surface film and to promote the rapid formation of surface films capable of reaching near-zero surface tensions under repetitive cycling [8]. Both peptides are highly hydrophobic and amphipathic. SP-C contains palmitoyl chains on cysteine residues 5 and 6 [9]. SP-B contains seven cysteines, which form three intramolecular disulfide bridges and an intermolecular one leading to the formation of a homodimer [10]. SP-B contains more polar and hydrophilic residues than SP-C and is therefore less hydrophobic. The tertiary structure of SP-B is unknown; however the structure is known for the 25-residue N-terminal fragment ($SP\text{-}B_{1-25}$), which is thought to retain most of the functionality of the full-length protein.

As the monolayer is compressed from a high molecular area to a low molecular area (low surface pressure to high surface pressure) it passes through distinct regions of the pressure area isotherm: G, LE + G, LE, LC + LE, LC [11]. In the gas (G) phase the lipids are very sparse and behave like a 2D gas [12]. The liquid-expanded (LE) phase is characterized by a fluid-like structure, where the molecules are in close contact with one another, but the lipid tails are conformationally disordered and contain a significant number of gauche configurations [12]. The liquid-condensed (LC) phase is a 2D semi-crystalline phase, which is characterized by hexagonal packing, lipid tails in the all-trans conformation with a substantial drop in the number of gauche defects, and decreased lateral mobility [12]. The formation of the LC phase results in the lengthening of the chains and thus a thicker monolayer. Upon compression the monolayer passes through two regions of phase coexistence (LE–G and LC–LE). In this paper, we will focus on LC–LE phase transitions at low surface tension (high surface pressure). Physiologically relevant surface tensions are in the range of 0–22 mN/m [5]. In mixed lipid and lipid–peptide monolayers, portions of the monolayer remain in the LE phase at these high surface pressures. In fact, LC and LE coexistence can persist in surfactant films at near-zero surface tensions and during reversible partial collapse transitions [13]. Several experimental studies have provided clear microscopic evidence of the coexistence of LC and LE phases in model surfactant monolayers, proving the existence of both micro-scale and nano-scale domains [4,14–18].

It is not fully understood how monolayers respond to the large changes in surface area, which occur during breathing. Neither the structural transitions involved nor the roles of each surfactant component are entirely clear. For example, the mechanism by which lung surfactant is able to avoid irreversible collapse under near-zero surface tensions remains a matter of great debate. The ability of lung surfactant to be rigid enough to sustain near-zero surface tension and yet fluid enough to respread rapidly, seems contradictory. This dichotomy, has lead to classical "squeeze-out" theory [19–21], which suggests that as the monolayer undergoes compression the surface is refined by the selective squeeze-out of non-DPPC components leaving behind a monolayer highly enriched in DPPC. Squeeze-out theory has since been refined to incorporate the existence of a peptide-promoted surface-associated surfactant reservoir, in which squeezed-out material can be stored for respreading upon expansion [22,23].

Recently, alternative theories have been proposed, such as the theory of "supercompression" [24–27]. It is known that to reach the near-zero surface tensions existing in the lungs the alveolar lining must compress past the equilibrium spreading pressure, and is thus by definition meta-stable. The effective viscosity of the alveolar film controls the rate at which the film flows into the bulk phase in response to the thermodynamic driving force [26]. It is therefore thought that to avoid collapse the monolayer must undergo a transition to a highly viscous material. According to Hall and co-workers [24–27] this can be achieved by the transformation of the monolayer into either a solid-like LC phase, as suggested by classical "squeeze-out" theory, or into a super-compressed fluid phase. Hall and co-workers have shown that both calf lung surfactant extract (CLSE) monolayers and monolayers of the pure POPC (an unsaturated phospholipid) can reach near-zero surface tensions if compressed quickly enough (super-compression) [24–27]. Such a super-compressed fluid maintains the high disorder of the fluid phase, but attains the resistance to flow that characterizes a solid.

In a recent review, Zuo et al. [2] provide an alternative interpretation of supercompression, suggesting that rapid compression facilitates the formation of nanodomains rather than microdomains, which take longer to assemble. It has been suggested that the finely divided nanodomain structure may act as an alloy or composite material, imparting both flexibility and stability to the film [2,4]. Furthermore, the nanodomain structure may enhance the homogeneity of partial collapse, which is initiated at domain boundaries [4]. Such partial collapse structures could provide additional stability to the surfactant film [2].

In order to begin to address the fundamental uncertainties regarding lung surfactant mechanics, an understanding of the interfacial structure of model surfactant mixtures is necessary. The phase state of a surfactant monolayer will determine the mechanical properties of the monolayer, and thus how the monolayer responds to the dynamic compression and expansion cycles occurring during respiration. The mechanism of collapse depends on the phase morphology, which is determined by the temperature, surface pressure, composition, and compression rate. For example, Gopal and Lee [28] showed that for a 7:3 DPPC/POPG monolayer at low temperatures (below 28 °C) the monolayer is biphasic and collapses by forming reversible large-scale folds (up to millimeters in length), while at high temperatures (above 33.5 °C) the monolayer is homogenous and collapses by forming micron-scale vesicular structures, and at intermediate temperatures (28–33.5 °C) collapse occurs by forming both folds and vesicles. Lee and co-workers [29–31] suggest that coexistence of LC and LE phases is an essential feature required for reversible collapse via a macroscopic folding transition. They propose that the coexistence of LC and LE phases provides the monolayer enough flexibility to bend and enough cohesiveness to prevent loss of material to the subphase. Partial collapse transitions in phospholipid monolayers also appear to require the coexistence of the LC and LE phases [29,32].

The composition of the film tunes the phase behavior. ARDS is associated with a change in the composition of LS resulting in surfactant inhibition. ARDS is often associated with the leakage of serum proteins into the lungs following lung injury [33–35]. An increase in cholesterol concentration can also inhibit lung function; see [36] and references therein.

Because the phase (or phase coexistence) of the monolayer determines the properties of the monolayer such as minimum surface tension, collapse mechanism, reversibility of collapse, and respreadability of the monolayer upon expansion, an understanding of how lung surfactant components affect phase behavior at high surface pressures is important to the rational design of surfactant replacements. To this end, here we study LC–LE phase transitions for DPPC monolayers and monolayers of DPPC with additional LS components. Previous CG-MD simulations have studied the role of surfactant components on the collapse behavior of disordered monolayers [37].

Historically, lipid phase transitions have proven difficult to simulate, requiring length and time scales not attainable by atomistic simulation. However, recent papers [38,39] have shown that it is possible to simulate the formation of small LC nuclei via atomistic simulation. Such simulations are computationally expensive however. Therefore, these simulations have been limited to pure DPPC monolayers and to relatively short time scales, preventing the study of the phase transition process in much detail.

In recent years, the development of coarse-grained models has allowed the simulation of longer length and time scale events. One popular CG force field, the MARTINI model [40,41], is parameterized

based on thermodynamic data and has been successfully applied to the simulation of a wide variety of lipid and lipid/peptide systems, some of which are discussed in a recent review [42]. Another notable CG force field was recently developed by Shinoda et al. [43]. This force field gives a pressure-area isotherm for DPPC monolayers closely resembling the experimental isotherm of Crane et al. [44] and successfully reproduces liquid crystalline bilayer properties such as area per lipid, area expansion modulus, and molecular distributions providing excellent agreement with experiment and atomistic simulation results. Shinoda et al. further demonstrated the utility of the CG-MD approach by performing simulations of bilayer self-assembly, monolayer collapse, and vesicle formation [43]. For a review of additional coarse grained models applied to lipid systems see [42].

Utilizing an early version of their MARTINI force field [45], Marrink et al. [46] applied CG-MD to the study of gel–liquid-crystalline phase transitions in DPPC bilayers. The line tension estimated with the MARTINI model was found to be in good agreement with the experimental value, and gel and fluid lateral diffusion rates from MARTINI were within the rather large error bars (factor of 10) of experimental estimates [46]. This work showed that the MARTINI model could successfully be applied to the study of lipid phase transitions. A recent study by Laing et al. [47] applied the MARTINI model to the simulation of 8:2:1 and 4:1:4 DPPC:POPG:cholesterol monolayers at 310K and surface tensions of 0, 20, and 40 mN/m. Although this study reported evidence of the formation of a condensed phase at elevated cholesterol concentrations, it was limited to small monolayers of 33–36 lipids each and did not focus directly on the phase transition process itself. The formation and coarsening of LC phase domains in DPPC monolayers have also been modeled using kinetic modeling [48]. To the best of our knowledge, MD simulation has yet to be applied to a detailed study of phase transitions in multicomponent lipid monolayers. Here we apply the MARTINI coarse-grained model [40,41] to the study of LE–LC phase transitions in DPPC monolayers, and phase transitions in mixed monolayers containing DPPC with additional lipid and peptide components. Although the MARTINI model has been found to exhibit unrealistic behavior at high areas per lipid [43], it gives reasonable results for densely packed interfaces as studied here.

In the LC phase DPPC molecules tilt at an angle of 25° with respect to the normal [12]. This tilt is due to a mismatch between the minimum cross-sectional area of 50 $Å^2$ for the head group and 38 $Å^2$ for both of the phospholipid tails combined [12]. For this reason the term tilted condensed (TC) is often used to describe the liquid condensed phase of monolayers containing DPPC. Although the tilted condensed phase is often discussed experimentally, all results reported here are for the untilted condensed phase. Because the MARTINI model implicitly incorporates some of the tail entropy of the lipid tails into the volume of the CG interaction sites, the DPPC molecules do not form the tilted condensed phase [46].

It has been suggested that non-equilibrium phase transitions should not be called “phase transitions”, but instead should be referred to as “phase transformations”. Since the terminology “phase transition” is in the experimental literature, we will therefore retain this terminology. However, it is important to note that the phase transitions observed here are distinctly non-equilibrium. Monolayers at high surface pressures (low surface tension) are in a metastable state and are thus inherently non-equilibrium structures. Furthermore, the true equilibrium between phases in the monolayer is established very slowly, as indicated by the dependence of experimental phase distributions on the rate of compression [4].

2. Simulation methods

The MARTINI CG model [40,41] was used in all simulations reported here. The CG mapping of DPPC, cholesterol, sodium ions, chloride ions, and water molecules is the same as that provided in the topology files on the MARTINI website [49]. The Perl script seq2cgtop_martini_v2.1tryout.pl [49] was used to generate the topology for coarse-grained SP-B_{1-25} and SP-C. The structure files for SP-B_{1-25} and SP-C were created by coarse-graining structure files for SP-B_{1-25} [50] and SP-C [51] that were obtained by FTIR and NMR spectroscopy. The MARTINI model is parameterized based on thermodynamic data, and has successfully reproduced membrane properties such as area per lipid [45,40], pressure-area isotherms [11], gel–liquid-crystalline phase transitions in bilayers [46], phase transitions between lamellar and non-lamellar phases [52,53], self assembly of bilayers, and structural and dynamic features of protein–lipid interactions [41]. Furthermore, the MARTINI model yields profiles of lateral pressure versus vertical position in the monolayer that are qualitatively similar to those obtained from atomistic simulations, suggesting that the MARTINI model captures the essential lipid/solvent properties [54].

Each configuration was constructed from two disordered lipid monolayers (each composed of 256 DPPC molecules) placed with heads facing each other across a layer of water, and tails separated by vacuum, in a periodic box, as described previously [11]. The z-dimension, normal to the layers, was adjusted to 100 nm, which allows more than enough space to prevent interaction of the tail regions of the two monolayers. In DPPC/SP-B_{1-25} monolayers, the SP-B_{1-25} molecules were then placed in each monolayer, oriented normal to the interface with the insertion sequence, which is the last eight residues on the N-terminus side, placed close to the head group region. During the first few nanoseconds of simulation, SP-B_{1-25} moves into the interface, and adopts a final orientation that is parallel to the interface, as observed previously [37]. Four peptides were inserted into each monolayer in three initial configurations: 1) with the peptides clustered together (not in contact, but with each peptide ~1.7 nm from the center of the box), 2) in a line (separated by ~3.3 nm), and 3) in a square (with each peptide placed ~4.5 nm from the center of the box). CG chloride ions were added to make the system electroneutral. The system was then energy minimized. In DPPC/SP-C monolayers, SP-C was placed in the monolayer in the line configuration as described above for SP-B_{1-25}, but with the α-helix placed initially embedded in the lipid tail region and tilted with respect to the interface. The SP-C molecules were initially placed differently that the SP-B_{1-25} molecules to account for differences in the experimental orientation of the two peptides in DPPC monolayers. SP-B is thought to reside near the headgroup region with its α-helix parallel to the interface [55]. However, SP-C is highly hydrophobic and infrared reflection–adsorption spectroscopy has revealed that SP-C adopts a tilted orientation, embedded within DPPC monolayers [56]. The simulated peptide concentrations were roughly 6 and 8 wt.% for SP-B_{1-25} and SP-C, respectively.

The CG topology and structure files for POPC were adapted from the lipid topology and palmitoyloleoylphosphatidylethanolamine (POPE) bilayer CG structure files taken from the MARTINI website [49], by replacing the ethanolamine head group bead (Qd) with a choline head group bead (Q0). A system containing two POPC monolayers was constructed in the same way as described above for the DPPC monolayers. Then to create 1:1 DPPC:POPC monolayers, POPC molecules were randomly replaced with DPPC molecules to obtain a 1:1 mixture and the system was then energy minimized. To create the DPPC/cholesterol monolayers, 50 cholesterol molecules were randomly inserted into each DPPC monolayer and the system was then energy minimized. The resulting monolayer contained roughly the same proportion of cholesterol to DPPC as in lung surfactant and was ~9 wt.% cholesterol. The topology used for cholesterol is the same as that reported on the MARTINI website [49]. The CG structure file for cholesterol was created by coarse-graining the first of eight atomistic structures for cholesterol (molecule A) obtained via X-ray diffraction by Shieh et al. [57].

For all simulations, temperature was maintained by coupling to a Berendsen thermostat [58] with a 1 ps time constant. Berendsen pressure coupling was used with a 1 ps time constant and all compressibilities set to 5E−6 bar^{-1}. Pressure was coupled anisotropically to 0 bar in all directions (zero surface tension). The surface tension is calculated from the following equation [59]:

$$\gamma(t) = \frac{L_z}{2}\left(P_{zz}(t) - \frac{P_{xx}(t) + P_{yy}(t)}{2}\right) \quad (1)$$

where t is time, L_z is the length of the box in the z-direction, and P_{xx}, P_{yy}, and P_{zz} are the pressures in the x, y, and z directions. As noted previously [37], due to pressure fluctuations the actual time-average surface tension differs slightly from this set point. For more details on each coupling mechanism the reader is referred to the GROMACS User Manual [60] and relevant simulation papers [61–65]. For all simulations, a timestep of 0.02 ps was used, and periodic boundary conditions were employed. All simulations were performed using GROMACS simulation software [66–68]. The following parameters were taken from the MARTINI website [49] and have been optimized for the coarse grained model: short-range electrostatic and van der Waals cutoffs of 1.2 nm, with van der Waals interaction shifting smoothly to Lennard Jones interaction at 0.9 nm. The neighbor list was updated every 10 steps using a grid with a 1.2 nm cutoff distance. In addition to the large computational speed-up, the molecular diffusivities of CG water and lipid molecules are around four times higher than for atomistic ones. As a result, the effective time of a simulation is roughly four times longer than the "physical" time [40]. However, all times reported here are physical times, as reported by the simulation.

After energy minimization the initial configurations (described above) were equilibrated for 1 μs at high temperature (338K for all peptide-free monolayers, and 333K for peptide-containing monolayers). The final configurations from these runs were used as starting states for 1 μs runs at low temperature (283K for all systems), to allow each monolayer to order. The final configurations of the high and low temperature runs were used as initially disordered and initially ordered starting configurations for subsequent runs, which were performed between 283K and 338K in 5K increments.

A program called Triangle was used to perform a Delaunay refinement on the simulation trajectories [69]. From the Triangle output files condensed phase lipids can be identified. The output files from Triangle were converted into an index file containing only the C2 tail sites that are considered to be in the liquid-condensed phase. Marrink et al. developed the following criteria: in order to be in the condensed phase (gel phase for bilayers) the C2 tail sites of a lipid must be six coordinated, corresponding to hexagonal packing, and must have five of its six neighboring C2 sites less than 0.75 nm away [46]. The second criterion is used to eliminate lipids that are six coordinated, but deviate considerably from hexagonal packing [46]. We used the same criteria in our analysis, except we tightened the second restraint to require that all six C2 sites be within 0.75 nm. This was done to limit noise in our data, which appeared as a few isolated C2 sites. In monolayers containing DPPC and POPC, the C2 sites of both phospholipids were used in the calculation of the percentage of hexagonally packing. In monolayers containing cholesterol, the R3 beads of the cholesterol molecules are treated as neighboring C2 sites in order to determine the extent of hexagonal packing for DPPC. However, the reported percentage of hexagonal packing is only calculated for the C2 sites of the phospholipids. The R3 beads of cholesterol were chosen as neighboring sites for the hexagonal packing analysis because they lie in the roughly the same xy-plane as the C2 sites of DPPC.

The simulation trajectories of the 1 μs runs were saved for packing analysis every 1 ns. Shorter (100 ns) runs are also reported for DPPC monolayers to assess artifacts attributed to simulation time. To allow more data points for packing analysis, the trajectories of these shorter runs were saved for packing analysis every 0.2 ns. The percentage of hexagonal packing was averaged between 500 ns and 1 μs for the 1 μs runs and between 50 ns and 100 ns for the shorter runs. For the longer time-scale runs there are a couple of cases where the transition from disordered to ordered phase or vice-versa occurs late in the simulation (after 500 ns); for these runs the hexagonal packing was averaged after the transition was complete, between 900 ns and 1 μs. The error bars reported on the hysteresis loops represent the standard deviation.

The simulations of DPPC monolayers yielded a large hysteresis loop with respect to temperature. In order to estimate the true transition temperature and study the growth of the ordered and disordered phases, the final configurations resulting from 1 μs simulations of initially ordered and initially disordered DPPC monolayers at 308K were merged together. As the monolayers condense the lateral dimensions of the monolayer decrease and the thickness increases. This transformation results in a thicker (larger in the z-dimension) water subphase in the system containing ordered monolayers. Therefore, to allow the ordered and disordered monolayer to align, a small water box containing 993 CG water molecules was inserted in the disordered box between the top monolayer and the original water subphase. The disordered and ordered boxes were then placed side by side in the x-dimension. A small ~0.7 nm mismatch between the monolayers in the y-dimension remained. To account for this mismatch two different systems were constructed, which we will call Merge1 and Merge2. In Merge1 the dimensions of the disordered box were shrunk by 0.7 nm, effectively compressing the disordered box slightly. Another configuration (Merge2) was generated where the larger y-dimension was kept, effectively disrupting the packing in the ordered system along the edge of the box where 0.7 nm of empty space is added. These systems containing side by side ordered and disordered regions were energy minimized and run at temperatures falling within the region of hysteresis (between 303K and 323K) for 100 ns. The coordinates were output to the trajectory every 10 ps to allow the growth or disappearance of the condensed phase to be captured in greater detail.

3. Results and discussion

3.1. Phase transitions in DPPC monolayers and binary monolayers containing DPPC

Here we investigate ordering and disordering transitions in DPPC monolayers and binary monolayers composed of DPPC with SP-B_{1-25}, POPC, and cholesterol. For each monolayer, 1 μs simulations were performed at high (338K for all peptide-free monolayers, and 333K for peptide-containing monolayers) and low (283K) temperature. The resulting ordered (LC) and disordered (LE) configurations (after 1 μs) were used as the starting states for subsequent simulations. Simulations were then run between 283K and 338K in increments of 5K from both disordered and ordered starting configurations. The disordered starting configurations contain a few isolated sites and small patches that meet the criteria of being hexagonally packed (Fig. 1, top). However, these isolated "ordered" sites do not constitute a true ordered phase. It should also be noted that within the simulation time-scale the monolayers do not become fully ordered. There are small defects in the packing (disclinations) even in the ordered starting configurations obtained after 1 μs at 283K (Fig. 2, top).

As the temperature is decreased from the disordered (high temperature) starting state to lower temperatures the formation and growth of the condensed phase are evident (Fig. 1). At a system-dependent temperature the LE–LC phase transition occurs. At the transition temperature, each monolayer displays the coexistence of ordered and disordered patches after 20 ns of simulation (Fig. 1, middle), and the existence of a defect-containing LC phase at the end of

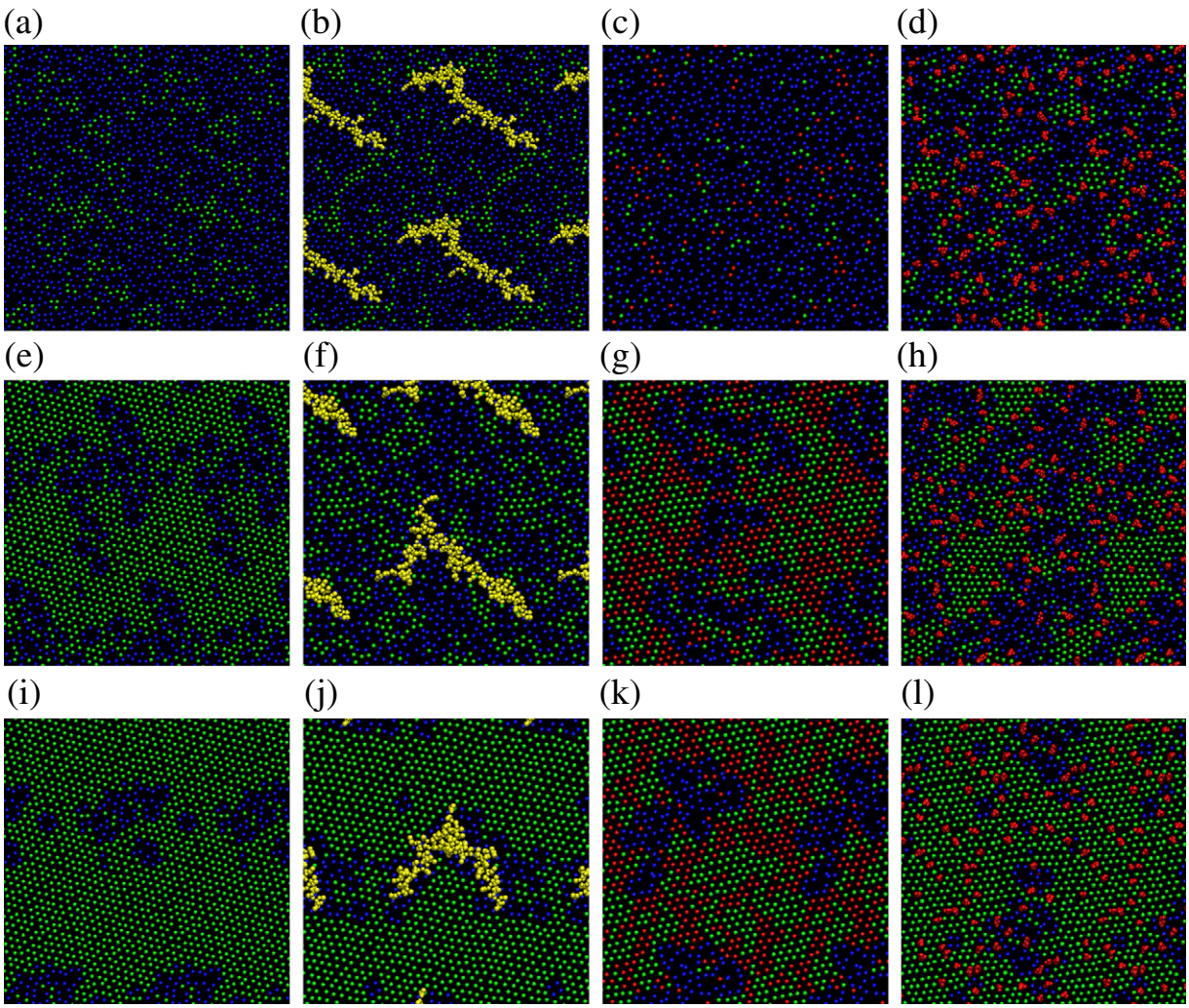

Fig. 1. Ordering phase transitions in DPPC, DPPC/SP-B_{1-25}, DPPC/POPC, and DPPC/cholesterol monolayers (from left to right) quenched from high temperature initially disordered monolayers. The monolayers shown are quenched to the following temperatures: DPPC (303K), DPPC/SP-B_{1-25} (303K), DPPC/POPC (283K), and DPPC/cholesterol (313K). The snapshots shown correspond to 0 ns (top), 20 ns (middle), and 1 μs (bottom). Ordered phospholipid C2 sites are shown in green, disordered phospholipid C2 sites are shown in blue, peptides are shown in yellow, and cholesterol is shown in red. In 1:1 DPPC/POPC monolayers all disordered phospholipid C2 sites are shown in blue and ordered phospholipid C2 sites are shown in green (DPPC) and red (POPC). This coloring scheme is also used in subsequent figures. In each system, both the top and bottom monolayers behave similarly. For clarity, only one monolayer is shown in each snapshot, with periodic images included.

the 1 μ s simulation (Fig. 1, bottom). At 303K the DPPC monolayers (Fig. 1, left), undergo a transition to the LC phase. The DPPC/SP-B_{1-25} monolayers are also observed to undergo an ordering transition at 303K (Fig. 1, center left). Here, the peptides loosely aggregate and localize within a single LE phase domain. Away from the peptides the monolayer is in the LC phase with a few small defects. In 1:1 DPPC:POPC monolayers, due to the high concentration of unsaturated phospholipid the ordering transition is observed at lower temperatures. When an initially disordered 1:1 DPPC:POPC monolayer is quenched to 283K (Fig. 1, center right), the monolayer orders and a single patch of LE phase remains (along with its periodic replicas in Fig. 1). Once ordering occurs, the LC phase consists of both DPPC and POPC, in similar proportions. Within the LC phase some separation between the two components is evident, the saturated (green) and unsaturated (red) components cluster together, but do not completely demix. We did not observe any segregation of the DPPC and POPC within the LE phase. Upon the reduction of the temperature to 313K, DPPC/cholesterol monolayers (Fig. 1, right) order with small patches of LE phase remaining at the end of the simulation. Cholesterol packs well within the LC phase and does not perturb the packing of the surrounding lipids. Cholesterol also appears to exhibit a preference for the interface between disordered and ordered lipids.

To examine the disordering transition the temperature is increased for each monolayer starting from a low temperature ordered state with defects (Fig. 2). As the temperature is increased to 323K, the pure DPPC monolayers undergo a transition to the LE phase with isolated LC patches remaining (Fig. 2, left). A similar transition is observed in DPPC/SP-B monolayers at 308K (left center), 1:1 DPPC:POPC monolayers at 298K (right center), and DPPC/cholesterol monolayers at 328K (right). In all of the monolayers the transition to the LE phase appears to occur by melting originating from defects in the monolayer. In other words, the small disordered regions of the monolayer, such as those associated with the presence of nearby peptides, grow at the cost of the surrounding LC phase lipids. In the DPPC/cholesterol monolayers, cholesterol shows a clear preference for the interface over the disordered phase. Even when there is more LE phase present, cholesterol is rarely surrounded entirely by disordered lipids, but instead tends to reside at the interface between ordered and disordered lipids.

In Fig. 3, the side views of LE (a) and LC (b) phase DPPC monolayers are shown. The ordering transition leads to longer, straighter chains and thus a thicker monolayer. From Fig. 3(b), the alignment of the chains in the LC phase, due to hexagonal packing, is clearly visible. For brevity only pure DPPC monolayers are shown.

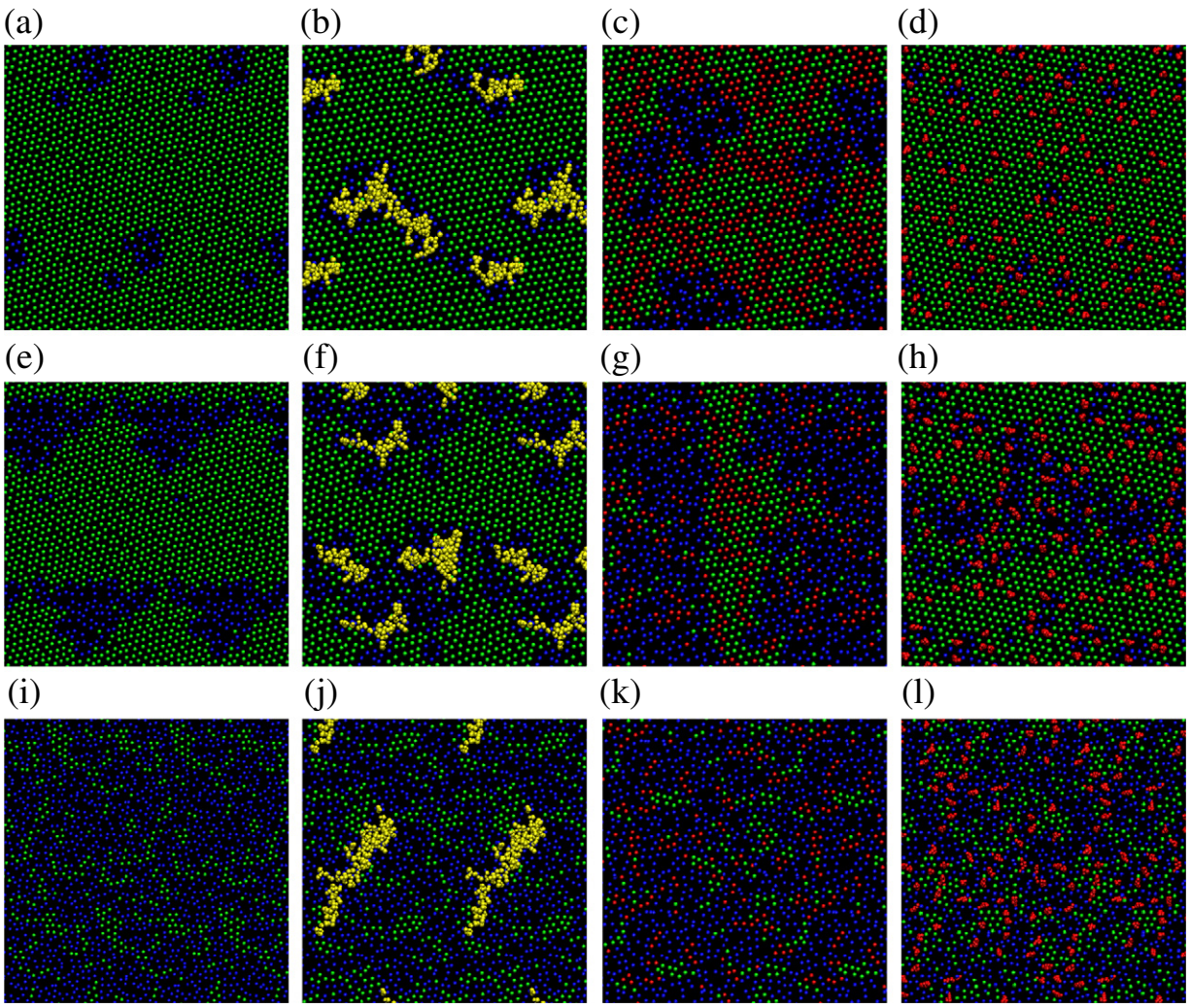

Fig. 2. Disordering phase transitions in DPPC, DPPC/SP-B_{1-25}, DPPC/POPC, and DPPC/cholesterol monolayers (from left to right) started from low temperature initially ordered monolayers. The monolayers shown are run at the following temperatures: DPPC (323K), DPPC/SP-B_{1-25} (308K), DPPC/POPC (298K), and DPPC/cholesterol (328K). The snapshots shown correspond to 0 ns (top), intermediate time (middle), and 1 μs (bottom). Intermediate snapshots were taken at 700 ns, 100 ns, 840 ns, and 220 ns for the DPPC, DPPC/SP-B_{1-25}, DPPC/POPC, and DPPC/cholesterol monolayers, respectively.

Mixed monolayers show similar structural changes with the LC–LE transition.

3.2. Hysteresis loops

For each simulation, the percentage of hexagonal packing was averaged between 500 ns and 1 μs, with data sampled every 1 ns, and graphed versus temperature in order to obtain hysteresis loops (Fig. 4), where a 1 μs run was performed at each temperature of the hysteresis loop. In each system, the results for the top and bottom monolayers were averaged together. The hysteresis loops obtained for the DPPC monolayers are compared to the hysteresis loops obtained for DPPC/SP-B_{1-25} (a), DPPC/POPC (b), and DPPC/cholesterol (c) monolayers.

In the pure DPPC monolayers phase transitions are observed between 303K and 323K. This range of temperatures is consistent with the experimental main phase transition temperature for DPPC bilayers of 314K [5]. In the pure DPPC monolayers, the originally disordered system orders between 308K and 303K and the originally ordered system becomes disordered between 318K and 323K. Comparing the observed ordering and disordering transition temperatures of pure DPPC monolayers, substantial hysteresis is evident. This hysteresis is decreased by the addition of a second component. While

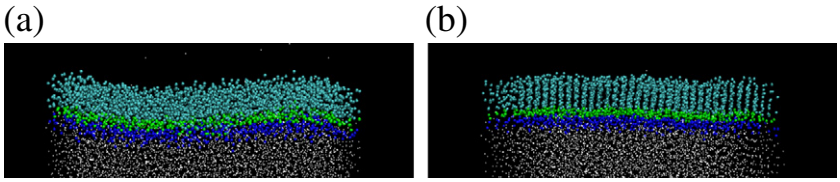

Fig. 3. A side view of disordered and ordered DPPC monolayers. The snapshots shown were taken after initially disordered monolayers were run for 1000 ns at 338K (a) and 303K (b). The DPPC tails, headgroups, and glycerol linkages are shown in turquoise, dark blue, and green, respectively. CG water molecules are shown as small white dots.

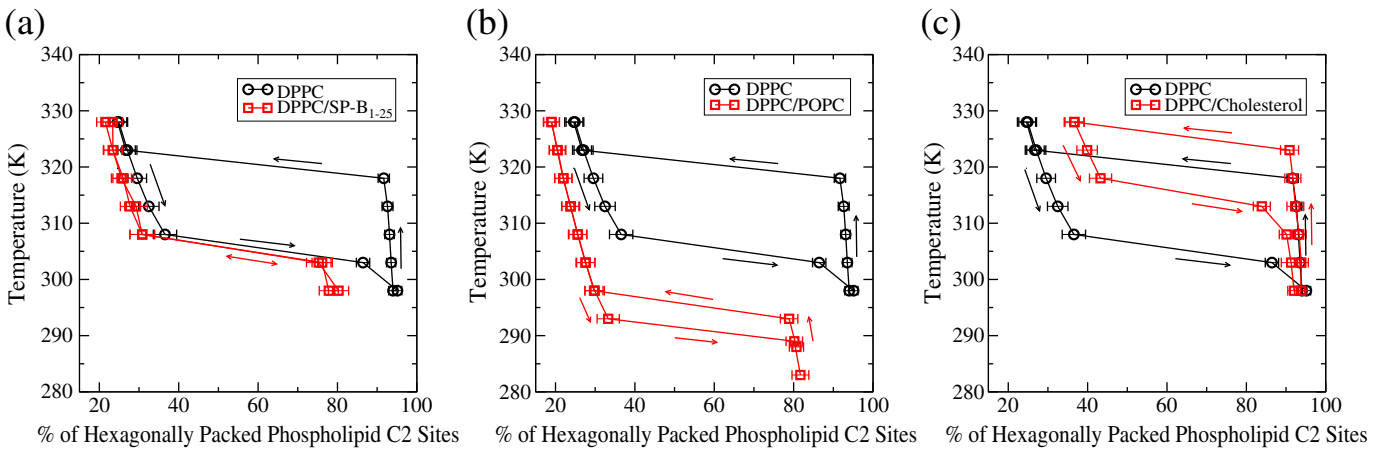

Fig. 4. Hysteresis loops showing the change in the percentage of hexagonally packed phospholipid C2 tail sites versus temperature for monolayers composed of DPPC (black circles) and monolayers composed of binary mixtures of DPPC with another lipid or peptide component (red squares). The binary mixtures consist of: DPPC/SP-B_{1-25} (a), DPPC/POPC (b), and DPPC/cholesterol (c). The error bars shown represent the standard deviation in the percentage of hexagonal packing at each point.

the addition of cholesterol or POPC decreases the hysteresis loop, the addition of SP-B_{1-25} abolishes the ordered side of the hysteresis loop altogether (Fig. 4(a)). This suggests that SP-B_{1-25} effectively nucleates disorder in the monolayer. In addition, SP-B_{1-25} also perturbs the packing of the surrounding phospholipids, shifting the ordered side of the hysteresis loop to lower percentages of hexagonal packing.

In Fig. 4(b), the addition of POPC to DPPC monolayers to create a randomly mixed 1:1 monolayer, leads to a substantial drop in the hysteresis loop to lower temperatures (288–298K). This result is not surprising, since unsaturated phospholipids have low transition temperatures in comparison to saturated phospholipids. Pure POPC bilayers have a main transition temperature of ~270K [70]. Thus, the transition temperatures observed here fall between the main transition temperatures of pure DPPC and pure POPC bilayers. On the length and time-scales of the simulations reported here, the presence of POPC spread throughout the monolayer prohibits the DPPC condensed phase domains from nucleating at higher temperatures. Once the ordered phase forms, both DPPC and POPC condense in similar proportions. After the LC phase forms, a larger amount of LE phase remains in the 1:1 DPPC: POPC monolayers than in the pure DPPC monolayers as evident by the shift in the ordered side of the hysteresis loop to lower percentages of hexagonal packing.

In Fig. 4(c), the hysteresis loop for DPPC/cholesterol monolayers has shifted up slightly (323–328K) compared to the hysteresis loop for pure DPPC, suggesting that the addition of cholesterol has resulted in an increase in the transition temperature and the stabilization of the ordered phase. In addition, the disordered region of the hysteresis loop becomes more ordered (shifts right) upon the addition of cholesterol. This suggests that the DPPC–cholesterol mixture is displaying a phase of intermediate order, which could be the so-called "liquid-disordered" (Ld) phase. There is no significant difference between the ordered sides of the hysteresis loops for DPPC and DPPC/cholesterol monolayers.

3.3. Area per lipid and transition temperature

The simulated LC phase DPPC monolayers reported here give areas per lipid near 0.48 nm^2/molecule, as reported previously [11]. This value falls within the range of experimental areas per lipid reported for gel phase DPPC bilayers of 0.479–0.523 nm^2/molecule [71] and agrees well with the reported range of experimental LE–LC plateaus in DPPC monolayers, but is larger than the limiting area of DPPC of 0.39 nm^2/molecule [72]; see reference [11] for review. This value is also comparable to the smallest values reported by Mohammad-Aghaie et al. [39] in their atomistic simulations of LC phase nucleation in DPPC monolayers, which were as low as 0.462 nm^2/molecule. The MARTINI model has also been reported to produce fluid phase bilayers with areas per lipid that are in agreement with experimental values [46]. An LE phase pressure-area isotherm [11] attained using an early version of the MARTINI model was found to agree well with an experimental LE phase isotherm obtained by Crane et al. [44] using the captive bubble apparatus. It is however problematic to compare simulated isotherms with experimental ones. Experimental isotherms can vary greatly depending on experimental conditions such as type of apparatus, spreading solvent, and compression rate, therefore complicating comparison of simulated and experimental isotherms; see reference [11] for review. However, for completeness some comparison is warranted. Therefore, the area per lipid was also calculated from the DPPC monolayer simulations, allowing isobars to be plotted. In Fig. 5(a) the simulated isobars are compared with the experimental isobars of Crane et al. [44] at surface pressures of 10, 40, and 65 mN/m. The simulated isobars agree well with the 40 mN/m experimental isobar, which falls in the middle of the simulated hysteresis loop. The surface tension of water measured by the MARTINI model is 30 mN/m [40], which is much lower than the actual surface tension of water. If we use the surface tension of water calculated by the MARTINI model the surface pressure in our zero surface tension simulations would correspond to 30 mN/m. Therefore, the similarity between our simulated isobars and Crane's 40 mN/m isobar is reasonable. In Fig. 5(b) the simulated DPPC and DPPC–cholesterol isobars are compared. The DPPC–cholesterol isobars are shifted to lower molecular areas than the DPPC isobars, with a relatively small deviation in the LC region and a larger deviation in the LE phase. This result agrees qualitatively with the observations reported by Blume and Hillmann for DMPC and DMPC cholesterol monolayers [73], which show a decrease in area per molecule with increasing cholesterol concentration with a much larger change in the molecular area for the LE phase than the LC phase. The observed behavior can be explained by a combination of the relatively smaller size of cholesterol, which shifts the area per lipid down for both the LE an LC phases, and the condensing effect of cholesterol on the LE phase.

It was found that for DPPC bilayers the macroscopic transition temperature estimated using the MARTINI model was 295 ± 5K [46], which is lower than the experimental phase transition for DPPC bilayers of 314K [5]. However, DPPC and DMPC are modeled the same in the MARTINI model, due to the coarse grained nature of the model, and the temperature observed in the simulations falls between the experimental transition temperatures of DPPC and DMPC. In monolayers the phase transition temperature depends not only on composition, but also on

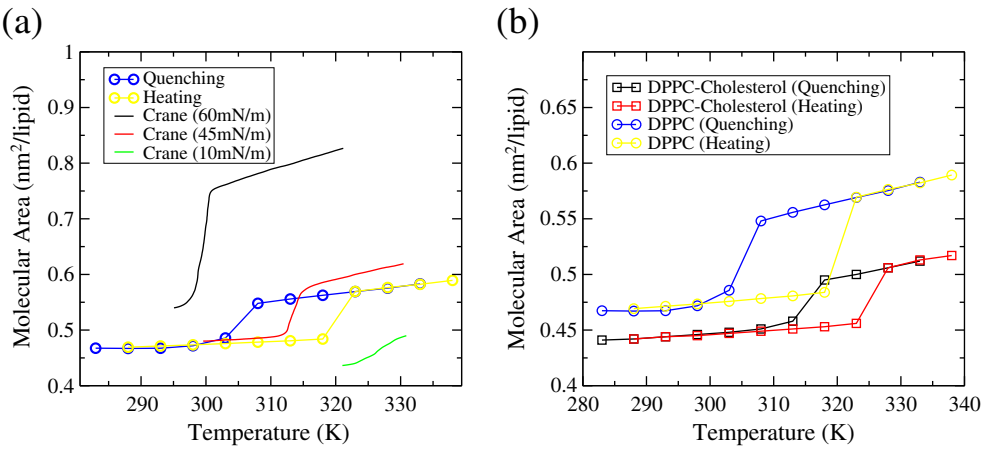

Fig. 5. DPPC and DPPC/cholesterol isobars. (a) Isobars obtained from the DPPC monolayer simulations reported here are compared to experimental DPPC isobars at surface pressures of 10, 40, and 65 mN/m. (b) Isobars are compared for simulated DPPC and DPPC/cholesterol monolayers.

surface pressure. Since a higher surface pressure favors a structure with lower molecular area, the transition temperature increases with surface pressure [26]. Melting temperatures of 321–328K have been reported by Yan et al. [26] for highly compressed DPPC monolayers; well above the main transition temperature of the bilayer. The melting side of the DPPC hysteresis loop reported here shows a transition between 318K and 323K, in good agreement with the experimental temperature range reported by Yan et al. However, consistent with previous DPPC bilayer simulations, the estimated macroscopic phase transition predicted from the simulated DPPC monolayers is lower than this experimental range. As the system size and simulation time are increased the ordered (melting) side of the hysteresis loop shifts to lower temperatures. As detailed later in this paper, the true (macroscopic) phase transition temperature is likely near 313K–315K.

3.4. Lipid components

In addition to DPPC, lung surfactant contains many other lipid components which are important to surfactant function. Unsaturated phospholipids, such as POPC, fluidize lung surfactant surface films, increasing adsorption to the interface and are thought to enhance respreading [1]. In lung surfactant, the ordered phase is thought to be enriched in DPPC and cholesterol, while the disordered phase is thought to be enriched in unsaturated phospholipids and surfactant proteins [7]. In the randomly mixed 1:1 DPPC:POPC monolayers studied here, substantial enrichment of either component in the LE (or conversely LC) phase is not observed. It appears that in the monolayers of 1:1 DPPC:POPC there are too many POPC molecules spread evenly throughout simulated monolayer to allow the DPPC molecules to nucleate a condensed phase region at temperatures above the point where POPC is also able to form a condensed phase. Therefore 1:1 DPPC:POPC monolayers undergo the LC–LE phase transition at much lower temperatures than the pure DPPC monolayers, with the monolayer remaining disordered at temperatures as low as 293K.

Within the LC phase some separation between the DPPC and POPC components is evident; the saturated (green) and unsaturated (red) components cluster together, but do not completely demix (Fig. 6). In contrast the LE phase always remains well mixed (not shown). In Fig. 6(b–d) radial distribution functions (RDFs) are given for an initially disordered monolayer quenched to 283K (corresponding to the system shown in Fig. 6(a)) for DPPC–POPC(b), DPPC–DPPC (c), and POPC–POPC (d). The height of the first peak is bigger in the DPPC–DPPC and POPC–POPC RDFs then in the DPPC–POPC RDFs, indicating a closer association of DPPC and POPC with themselves than with each other. The RDFs are averaged over five time intervals: 0–10 ns (blue), 10–50 ns (green), 50–100 ns (yellow), 150–200 ns (red), and 900–1000 ns (black). In all three RDFs, there is a clear increase in order and in the height of the first peak at later times compared to the first time interval (0–10 ns), but this increase quickly saturates at times beyond around 10 ns. However, in a larger system size simulation containing 1024 lipids per monolayer, at 283K, a larger domain of ordered POPC was evident (Fig. 7).

The observed coexistence between ordered DPPC and ordered POPC domains is not likely to be physiological, since POPC has a low transition temperature and is expected to be in the disordered phase at physiological temperatures. Given longer length and time scales, one would expect POPC and DPPC phase separation, allowing DPPC to condense without a substantial proportion of POPC also condensing. Although the simulation results reported here for DPPC/POPC monolayers are unphysiological, the addition of unsaturated phospholipids to membranes has been observed to reduce the transition temperature below that of pure DPPC [7], as observed here.

Cholesterol is another important component of lung surfactant, comprising about 5–10 wt.% of natural surfactant [7]. Experimental results show that the removal of cholesterol from native lung surfactant has a dramatic effect on the lateral structure and spreading properties of the lung surfactant film [74]. However, cholesterol is systematically removed from some surfactant replacements to enhance stability [7]. Conclusions about the role of cholesterol in surfactant function have been contradictory and a clear understanding of the cholesterol's role remains elusive. The effect of cholesterol on phase behavior appears to have a strong dependence on the composition, with both the amount of cholesterol present and the presence of additional components such as unsaturated phospholipids and surfactant having an effect. Also, phase behavior is known to depend strongly on experimental conditions such as rate of compression and the presence of ions. Thus, contradictory conclusions about the role of cholesterol are likely attributed in part to variation in experimental conditions. Although various theories have been proposed to explain the effects of cholesterol on the phase behavior of phospholipid bilayers and monolayers, it is generally accepted that cholesterol modulates the phase behavior of surfactant membranes by disordering phospholipids in the LC (or gel) phase and ordering phospholipids in the LE (or liquid-crystalline) phase, resulting in the formation of the so-called “liquid-ordered” (Lo) and “liquid-disordered” (Ld) phases, respectively [7]. Cholesterol decreases packing and increases the mobility of phospholipids in the ordered phase and reduces the conformational entropy of the phospholipid acyl chains in the disordered phase [7]. The Lo phase is more fluid then the LC phase, and the Ld phase is less fluid than the LE phase (LC<Lo<Ld<LE) [2,7].

The effect of cholesterol on lipid bilayers has been studied extensively. Some interesting simulation studies have shed some light on the behavior of cholesterol in bilayers. Early atomistic molecular

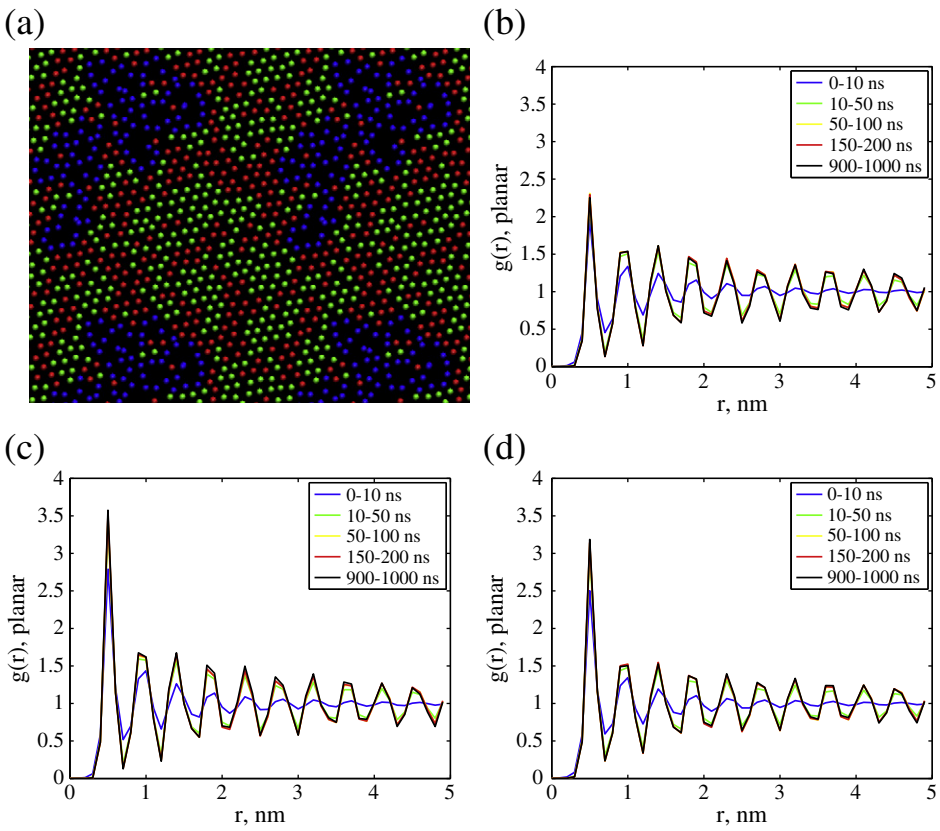

Fig. 6. Radial distribution functions. An initially disordered monolayer is quenched to 283K (a). The corresponding radial distribution functions are also shown for DPPC–POPC (b), DPPC–DPPC (c), and POPC–POPC (d) association. The RDFs are averaged from 0–10 ns (blue), 10–50 ns (green), 50–100 ns (yellow), 150–200 ns (red), and 900–1000 ns (black). The snapshot shown was taken after 1 μs of simulation at 283K.

dynamics simulations of a DPPC/cholesterol bilayer revealed a slight condensing effect of cholesterol on the bilayer resulting in a reduction in empty free volume and a significant influence of cholesterol on subnanosecond time-scale lipid dynamics including reduced center-of-mass rattling motion and reduced methylene reorientational motion along the entire length of the hydrocarbon chains [75]. In a more recent study, atomistic MD simulations revealed that in DPPC/cholesterol bilayers high concentrations of cholesterol (~20%) change the pressure profile across the bilayer from being relatively flat to an alternating sequence of large positive and negative lateral pressures [76]. Using a multi-state computer model Mouritsen and coworkers [77,78] found that cholesterol exhibited an ordering effect on disordered bilayers, a disordering effect on order bilayers, and displayed an affinity for domain interfaces. In addition, multi-scale simulations of lipid bilayers combining MD and mean-field theory showed that cholesterol induced structural changes in the bilayer by causing local ordering of the phospholipids around each cholesterol molecule [79]. Also, the MARTINI model has also been used to simulate phase transitions in a bilayer containing cholesterol with both saturated and unsaturated phospholipids [80]. These simulations showed the formation of coexisting liquid-ordered and liquid-disordered phases with structural and dynamic properties that closely matched experimental data. Studies of monolayers containing cholesterol are much less prevalent. Recent atomistic and CG simulations of small (33–36 lipids) 8:2:1 and 4:1:4 DPPC:POPG:cholesterol monolayers at 310K and low surface tensions reported that the addition of cholesterol resulted in a phase change of the monolayers from an expanded to a condensed phase [47]. Our observations agree well with previous simulation studies showing the condensing effects of cholesterol on disordered monolayers and bilayers [47,77–79], the localized ordering observed in phospholipids neighboring cholesterol [79], and cholesterol's affinity for domain boundaries [77,78]. Experimental studies have also revealed that cholesterol has a marked affect on domain shape and size due to its line active properties [81,82], which has been interpreted as a specific binding of cholesterol to the boundary region between condensed and fluid phases [81].

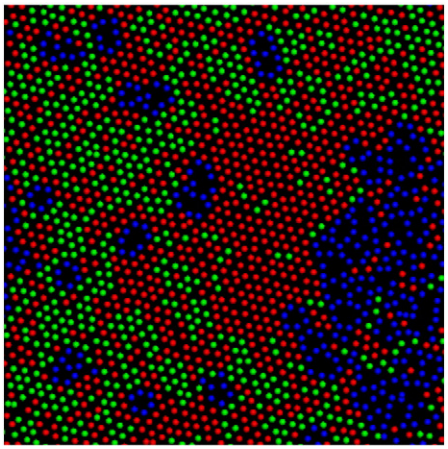

Fig. 7. A 1024 lipid 1:1 DPPC:POPC monolayer 1 μs after being quenched to 283K from a high temperature initially disordered state. This figure contains only a single periodic image, unlike the previous images.

In Fig. 8 snapshots are shown at selected temperatures with corresponding RDFs showing the distribution between cholesterol molecules and disordered C2 sites (blue), ordered C2 sites (green), and other cholesterol molecules (red). The RDFs confirm the observed preference of cholesterol to reside at the interface. The RDFs obtained from the ordered monolayers (Fig. 8(b)) demonstrate a stronger association of cholesterol with the disordered sites than with the ordered sites, as evident from the magnitude of the first peaks in the

radial distribution functions. In contrast the RDFs corresponding to disordered monolayers (Fig. 8(d)) demonstrate a stronger association of cholesterol with the ordered sites than with the disordered sites. The stronger association of cholesterol with disordered sites in a mostly ordered monolayer and with ordered sites in a mostly disordered monolayer reflects cholesterol's preference for the interface. In the disordered monolayers (Fig. 8(d)) the first peak in the cholesterol–cholesterol distribution is very weak, showing that cholesterol does not associate strongly with itself. In the ordered monolayers (Fig. 8(b)) the self-association increases, but remains relatively weak. It is interesting to note that the cholesterol–cholesterol RDF of the disordered monolayer (Fig. 8(d)), which contains a substantial fraction of isolated ordered patches, closely resembles the RDF reported for coexisting liquid ordered and liquid disordered phases in a CG bilayer modeled with the MARTINI force field [80]. Whether heating from low temperature or cooling from high temperature, little structural differences are seen between the RDFs of two disordered monolayers or between the RDFs of two ordered monolayers (not shown). The RDFs of the ordered monolayers show long-range order, while the RDFs for the disordered monolayers show a few well-defined peaks indicating some short-range order resulting from small patches of condensed phase.

3.5. Hydrophobic surfactant proteins

Our observations agree well with experimental observations of the influence of surfactant peptides on lipid packing. SP-B, SP-B_{1-25} and SP-C are known to localize within the fluid phase [14,17,29,30,74,83–91] and have been found to perturb monolayers of DPPC, DPPC/DPPG, and palmitic acid (PA), increasing the overall fluidity of the monolayers and producing smaller and more numerous condensed phase domains [14,17,29,83,92,85,86]. Fluorescence and scanning force microscopy report that SP-B affects the distribution of LE and LC regions of DPPC at both the microscopic and nanoscopic level causing an overall reduction in the total amount of LC phase present and an increase in the LC–LE interface [17]. It has therefore been hypothesized that SP-B promotes the formation of a fine nanoscopic framework of lipid and lipid–protein nano-domains, which may lend the film both structural stability and dynamic flexibility. SP-B has also been observed to segregate and form clusters at phase boundaries [17]. Our simulations show that SP-B_{1-25} perturbs the packing of the neighboring lipids. Also, the peptides tend to localize and aggregate within a single LE phase domain. The aggregation seen in our simulations agrees well with the experimental observation of SP-B clusters at domain boundaries. However, the domain sizes in our simulations are too small to say whether the SP-B aggregates prefer phase boundaries over the bulk LE phase.

To further evaluate the affect of the peptides on the monolayer, a larger system was generated from the disordered starting state by copying the box laterally to create a system containing four times as many molecules as the original system. After 1 μ s of simulation at 303K, these larger monolayers show a large amount of LC phase with some LE phase centered around the peptides. The peptides disrupt the crystallinity of the ordered phase and act as defects in the monolayer. In order to propagate the LC phase must grow into peptide-free regions of the monolayer, this growth essentially pushes the peptides together uniting them within the small fraction of disordered phase (Fig. 9). This type of behavior may explain why SP-B has been observed to aggregate experimentally. Furthermore, the fact that the peptide impedes the spread of ordered domain may explain, at least in part, why the peptides have been observed at domain boundaries. Simulations containing larger LE domains in coexistence with the LC phase, would help to provide more definitive results regarding the

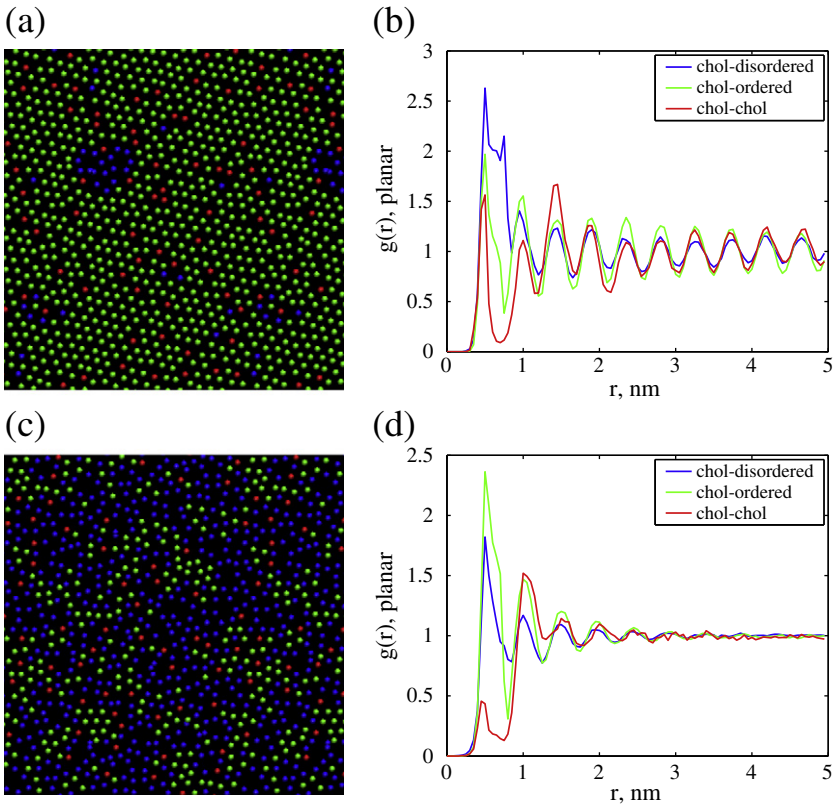

Fig. 8. Radial distribution functions for DPPC/cholesterol monolayers. Snapshots and corresponding RDFs of ordered (a,b) and disordered (c,d) monolayers are obtained for an initially ordered monolayer heated to 303K and 328K, respectively. In the radial distribution functions (c,d) the cholesterol-ordered C2 (green), cholesterol-disordered C2 (blue), and cholesterol–cholesterol (red) distributions are shown. The snapshots were obtained after 1 μs of simulation. The RDFs are averaged over the last 500 ns of simulation.

localization of the peptides at domain boundaries. However, such simulations would be computationally expensive and are not yet practical. From Fig. 9, it is apparent that the peptide-filled LE phase breaks up the condensed phase. This behavior is in consensus with the proposed role of SP-B_{1-25} in the formation of a fine nanoscopic framework.

3.5.1. Effect of initial position

To test the dependence of the domain formation on the initial position of the peptides, three different initial configurations were used. As described in the Simulation methods section, four peptides were placed partially inserted in each monolayer so that they formed a square, a line, and a cluster, with respect to each other. All snapshots in Figs. 1 and 2 correspond to the line initial configuration. In Fig. 10, the monolayers with the line (left) initial configuration are reproduced alongside corresponding simulations with the square (center) and cluster (right) initial configurations. The snapshots shown were taken after 1 μs of simulation for the line and square initial configurations and after 100 ns of simulation time for the cluster initial configuration. Note that the simulations involving the cluster initial configuration were limited to 100 ns because the onset of fold nucleation around the peptide aggregate limited access to longer simulation times. The observed fold nucleation has been discussed previously [37]. The snapshots shown were taken at 303K after quenching from a disordered state (top) and heating from an ordered state (bottom). The simulations with the square initial configuration result in similar amounts of LC and LE phase lipids as the line initial configuration. However, the amount of LC phase is slightly greater in the monolayer where the peptides were initially clustered together. These simulations show that condensed phase formation is perturbed by the insertion of peptides, and the extent of perturbation depends on the position of the peptides relative to one another. The peptides perturb the surrounding lipids, and therefore if the peptides are clustered together, the LC phase is only perturbed in the immediate vicinity of the peptide cluster and most of the LC phase is left unaffected. In fact, the total amount of LE phase lipids at 303K is roughly the same in the cluster configuration (Fig. 10(c) and (f)) as in the pure lipid system (Figs. 1 and 2). However, if the peptides are spread out (as is the case for the line and square starting states), the LE phase surrounds the peptides, covering more area and decreasing the total amount of LC phase present in the monolayer. Therefore, the growth of the LC phase favors the aggregation of the peptides.

3.5.2. Hydrophobic surfactant protein SP-C

A limited number of simulations were also performed for monolayers containing SP-C. To correspond with experimental observations, SP-C was placed initially tilted and embedded in the DPPC monolayer [56]. Using the line initial configuration, disordered and ordered starting states for DPPC/SP-C monolayers were generated in the same manner as the starting states for the DPPC/SP-B_{1-25} monolayers. Simulations were performed at 303K and 308K using both initially ordered and disordered starting states. At 303K both starting states resulted in ordered monolayers after 1 μs of simulation (not shown). However, hysteresis is evident at 308K. After 1 μs at 308K, the initially disordered monolayer remains disordered (Fig. 11(a)) and the initially ordered monolayer remains ordered (Fig. 11(b)). It is unclear why initially ordered DPPC/SP-C monolayers remain ordered at 308K, where DPPC/SP-B_{1-25} monolayers disorder (Fig. 2). To further elucidate this difference in phase behavior at 308K, the DPPC/SP-C (Fig. 11(c)) and DPPC/SP-B_{1-25} (Fig. 11(d)) monolayers are visualized from the side. This shows that SP-C penetrates deeper into the monolayer than does SP-B_{1-25}. However, the SP-B_{1-25} containing monolayer shows substantial deformation around the SP-B_{1-25} aggregate, resembling a pre-collapse instability. The observed difference in the phase behavior of the SP-C and SP-B_{1-25} containing monolayers may be linked to the curvature of the monolayer near the peptide, and requires further investigation beyond the scope of this paper.

It is also interesting to note that in Fig. 11(c), the palmitoyl chains of SP-C (shown in red) remain firmly embedded within the monolayer. It has been proposed that at high surface pressures (low surface tension) SP-C is partially squeezed-out of the monolayer with associated lipids, but remains anchored to the monolayer interface by its palmitoyl chains, which remain embedded within the monolayer [36,87–90,93,94].

3.6. Implications of phase behavior on partial collapse at high surface pressure

Classical squeeze-out theory predates knowledge of surfactant proteins. In recent years, squeeze-out theory has been revised to suggest the existence of a protein associated surfactant reservoir, which stores material removed from the interface upon compression near the interface where it is readily available for reinsertion upon expansion. Several studies have reported evidence of peptide associated partial collapse structures, which may act as reservoirs [4,29,30,83–97]. It should be noted that these studies do not necessarily suggest enrichment of the monolayer in DPPC, as suggested by classical squeeze-out theory. These protein partial collapse structures have been observed to originate from the LE phase [4,30,84–90]. In this work, lung surfactant peptides are clearly excluded from the condensed phase and reside within the fluid phase. This is consistent the appearance of peptide-associated partial collapse structures within the fluid phase. In a previous paper, we assessed the role of lung surfactant components on collapse [37]. One of the key findings of this paper is the peptide-mediated nucleation of small collapse structures, which are comparable to those identified experimentally. These results along with the results presented here paint a picture that is consistent with revised squeeze-out theory, and suggest an important role for SP-B and SP-C. The lungs surfactant proteins appear to act as a catalyst, destabilizing the

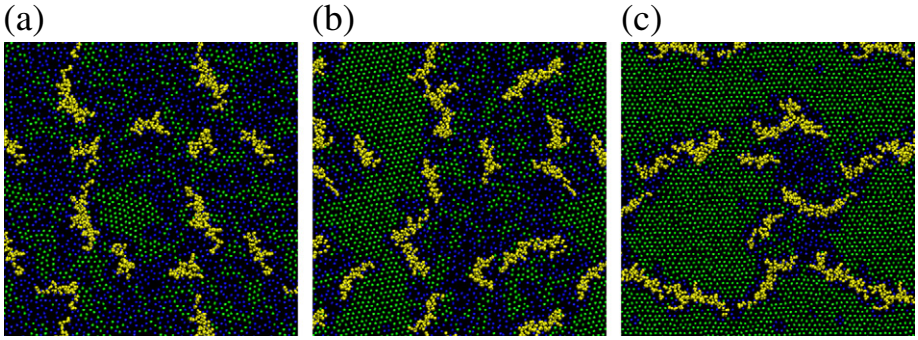

Fig. 9. Packing in monolayers composed of 1024 DPPC with 16 SP-B_{1-25} molecules. A high temperature initially disordered monolayer is quenched to 303K. The snapshots shown were taken after (a) 10 ns, (b) 100 ns, and (c) 1 μs of simulation time.

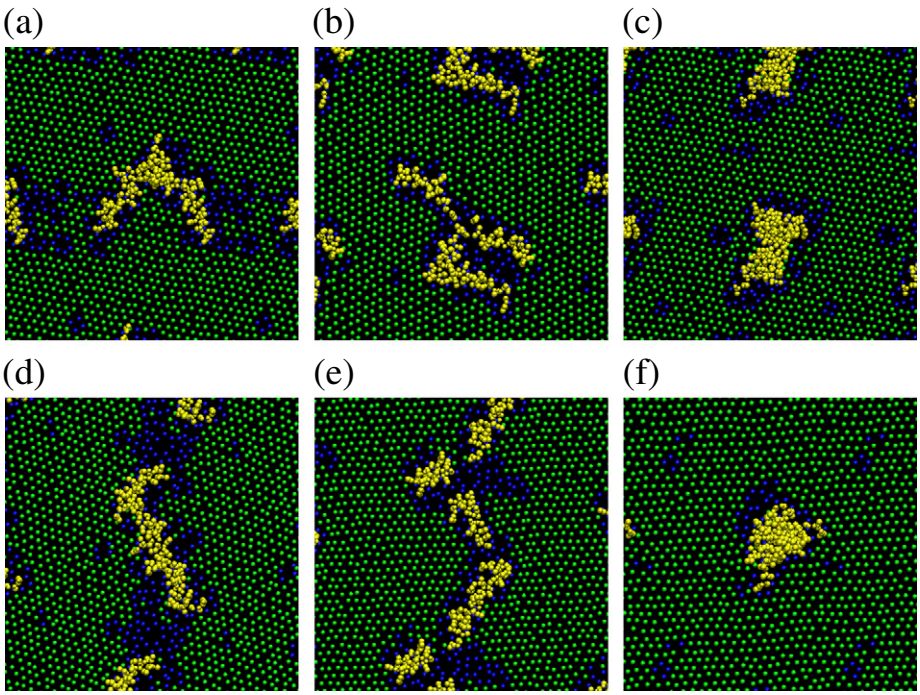

Fig. 10. The influence of peptide orientation on the LC–LE phase coexistence. Three peptide initial orientations were studied: line (left), square (center), and cluster (right). The snapshots were taken after 1 μs of simulation at 303K, with the exception of cluster configuration, which was taken after 100 ns of simulation time. The monolayers on the top were quenched from a disordered state and the monolayers on the bottom were heated from an ordered state.

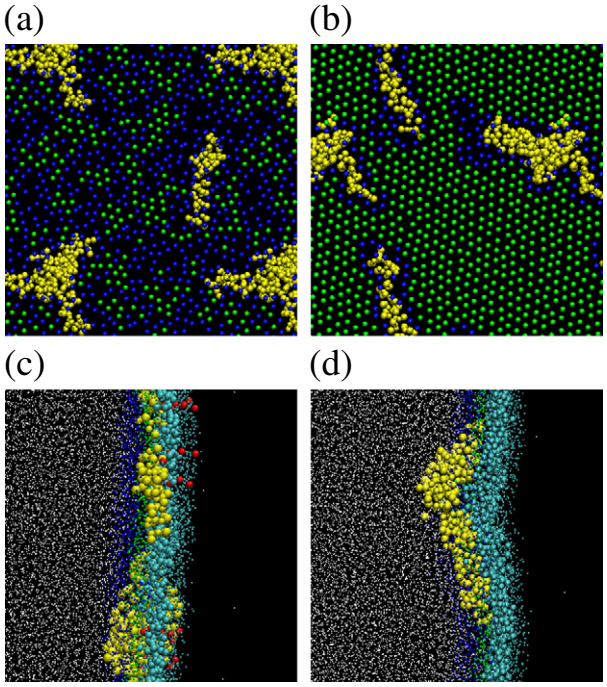

Fig. 11. The phase behavior of monolayers containing SP-C. After 1 μs of simulation at 308K, the initially disordered DPPC/SP-C monolayers remain disordered (a) and the initially ordered DPPC/SP-C monolayers remain ordered (b). Side views are also given to elucidate the difference between initially ordered SP-C (c) and SP-B_{1-25} (d) containing monolayers after 1 μs of simulation at 308K. In (c) and (d) the peptides are shown in yellow, the palmitoyl chains of SP-C are shown in red, and the CG water molecules are shown as small white dots. The DPPC tails, headgroups, and glycerol linkages are shown in turquoise, dark blue, and green, respectively. To clearly visualize the depth of the peptide penetration into the monolayer, the C2 sites of the phospholipid tails are enlarged with respect to the rest of the phospholipid sites.

monolayer and acting as a nucleation site for phase and collapse transitions.

It has been suggested that partial collapse structures should have the same composition as the phase from which they are formed [98]. The peptide enrichment of LE phase observed here and the known association between peptides and collapse structures both suggest that the collapse structures may be enriched in surfactant proteins. Collapse structures have also been observed to preferentially associate with domain boundaries [4]. This could suggest that components, which exhibit a preference for domain boundaries may also be enriched in the collapse phase. Here we observe a clear preference of cholesterol for the interface. This observation agrees with experimentally observed line-active properties of cholesterol [81,82]. If both cholesterol and collapse structures exhibit a preference for domain boundaries, the concentration of cholesterol would likely have a direct influence on the existence and number of partial collapse structures. In fact such and affect has been observed. In a recent experimental study revealed that the addition of 10 mol% cholesterol resulted in an increase in the number and size of protrusions [99]. However, large amounts of cholesterol (30 mol%), increased monolayer rigidity and prevented the formation of partial collapse structures. The direct influence of cholesterol on the existence and number of partial collapse structures may be attributed in part to the preference of both cholesterol and collapse structures for the interface.

We do not observe any evidence for supercompression. However, there are physiological complexities (i.e. structural changes and heterogeneous phase and composition) that are not fully accounted for by simulation. It remains unclear if the physiological stability of lung surfactant at high surface pressures is attributed to a combination of phase and partial collapse transitions or to supercompression.

3.7. Nucleation and growth and transition temperature

The 1 μ s simulations of DPPC monolayers lead to a large amount of hysteresis, with the LC–LE phase transition occurring between 303K and 323K. To obtain a better approximation of the true transition temperature of our DPPC monolayers, several simulations were run

where ordered and disordered monolayers were fused together as described in the Simulation methods section. In short, two systems were constructed, Merge1 and Merge2. To attain the proper alignment between the ordered and disordered systems, the disordered monolayer was condensed by 0.7 nm in the y-direction in Merge1 and in Merge2 the width of ordered box was increased by 0.7 nm in the y-direction. The starting configuration for Merge2 is shown in Fig. 12(a). The starting configuration for Merge1 (not shown) is visually similar to the configuration shown for Merge2. The extra space along the edge of the box in Merge2 leads to the disordering of the lipids along the edge of the box, which causes the size of the LC domain to shrink, see Fig. 12(b).

The construction of Merge1 and Merge2 established two systems with a well-defined front between the ordered and disordered phases, making them ideal systems for the study of the nucleation and growth of LC phase and also the melting of the LC phase. For example, in Fig. 12(a–f) the simulation of Merge2 at 310K is shown. Once the simulation is started, the size of the LC phase domain quickly shrinks (Fig. 12(b)) due to disordering of the lipids along the edge of the box associated with the introduction of extra space into this system. After the initial shrinkage, the ordered phase then begins to re-grow (Fig. 12(c,d)). After 60 ns (Fig. 12(e)) the ordered phase has propagated across the entire box and an LE phase domain becomes entrapped. After 100 ns (Fig. 12(f)) of simulation the LE phase domain has decreased slightly in size and additional defects are also present in the LC phase packing. Simulations were also run at 308K, 313K, and 318K for both Merge1 and Merge2 monolayers and at 315K for Merge1 monolayers. At 308K the monolayers in both systems (Merge1 and Merge2) order, while at 318K both systems disorder. At 313K the monolayers in Merge1 order but the monolayers in Merge2 disorder, suggesting that the critical nucleus for ordering is attained in Merge1 and not in Merge2. The disruption of the packing along the edge of the box in Merge2 likely causes the LC domain size to shrink below the critical nucleus size. At 315K the ordered region of Merge1 begins to grow into the initially disordered box (Fig. 12(g)), but then shifts so that roughly half of the disordered box becomes ordered and roughly half disordered (Fig. 12(h)). Packing fluctuations are evident, but the relative amount of LE and LC phases does not change significantly for the remainder of the simulation (Fig. 12(i)) suggesting that the coexistence of the condensed and expanded phases is stable on the time-scale of this simulation. These results suggest that the true transition temperature lies between 310K and 318K, and the behavior observed at 313K and 315K suggests that these simulations are in close proximity to the actual transition temperature.

These simulations show a nucleation and growth mechanism similar to that reported by Marrink and co-workers in their simulations of DPPC bilayers [46]. The LC phase domains are observed to fluctuate, shrinking and growing in size. At some point a critical nucleus is obtained and the ordered phase continues to spread. After the ordered phase propagates some disordered lipids become entrapped. Further ordering is slow and defects are long lived. Defect-free monolayers are not observed over the course of our 1 μ s simulations. As reported for DPPC bilayers [46], the defects are long lived because the freezing of trapped disordered domains requires global reorganization of the LC matrix.

In the reverse process, disorder originates from a defect in the monolayer such as a disordered patch of lipids around a peptide or near the edge of the box, where extra space was inserted into Merge2. The LE phase grows at the cost of the LC phase domain, which shrinks and eventually disappears. As shown in Fig. 4(a), the SP-B_{1-25} molecules are observed to nucleate disorder in the monolayer leading to the collapse of the hysteresis onto the disordered side of the hysteresis loop. This behavior may result from the high concentration of SP-B_{1-25} in our simulations, which could prevent the formation of a critical nucleus.

Given that the formation of liquid condensed domains involves a nucleation process, the large amount of hysteresis observed in our

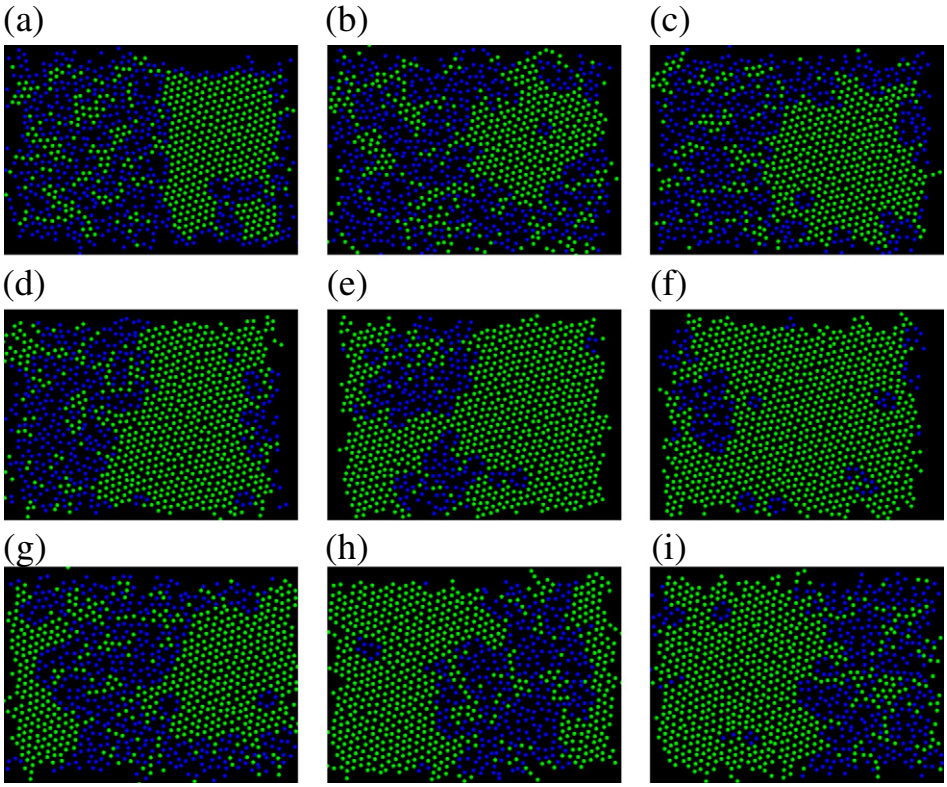

Fig. 12. Nucleation and growth of the LC phase. The starting configuration for Merge2 simulations is shown (a). Snapshots from the simulation of Merge2 at 310K are shown after 0 ns (a), 2 ns (b), 20 ns (c), 40 ns (d), 60 ns (e), and 100 ns (f) of simulation time. Snapshots from the simulation of Merge1 at 315K are shown after 14 ns (g), 60 ns (h), and 100 ns (i) of simulation time.

simulations is not surprising. Marrink et al. also observed significant hysteresis between melting and freezing transition temperatures for coarse-grained DPPC bilayers [46]. They suggest that the condensed phase can remain stable well past its transition temperature due to kinetic trapping.

3.8. Packing fluctuations

To quantify the persistent changes in packing caused by instantaneous domain patterns, we plotted the percentage of hexagonally packed sites versus simulation time (Fig. 13). Data for both the top (red) and bottom (black) monolayers are shown. The fluctuations in hexagonal packing typically fall in the range of ±2–5%. The error bars reported in Fig. 4 give the standard deviation in the percentage of hexagonal packing for DPPC, DPPC/cholesterol, DPPC/POPC, and DPPC/SP-B_{1-25} monolayers. These error bars thus reflect the magnitude of the packing fluctuations. From the size of the error bars and from Fig. 13 it is apparent that the fluctuations are a little bit larger in the disordered monolayers than in the ordered monolayers. Also, the fluctuations seen in the monolayers of pure DPPC do not differ greatly from those seen in monolayers composed of DPPC with cholesterol, POPC, or SP-B_{1-25}. However, the addition of a second component does result in slightly larger fluctuations in the LC phase monolayers. The magnitude of the fluctuations also increases slightly as the temperatures approach the transition temperature on either side of the hysteresis loop.

In most of our simulations, phase transitions occur within the first 500 ns of simulation. However, the monolayers are meta-stable, and long simulation times increase the probability of the development of a critical nucleus. Therefore, the size of the hysteresis loop is a function of simulation time. For DPPC monolayers at 323K the transition from LC to LE phase occurs after 700 ns of simulation time, as shown in Fig. 13. Both the top and bottom monolayers undergo the transition at the same time, due to coupling between the two monolayers, produced by the shrinkage of the lateral dimensions of the box that occur upon ordering.

The fluctuations observed in our simulations are analogous to hetero-phase fluctuations reported in lipid bilayers near the main transition temperature [46]. There are also a limited number of simulation studies discussing fluctuations observed in the phase transitions of monolayers. Using a multi-state computer model, Mouritsen et al. [100] found that thermally induced density fluctuations led to inhomogeneous micro-states and instantaneous lipid domain patterns in monolayers. They attribute the slow relaxation process to kinetic stabilization of the domain interfaces by intermediate conformational states, which lower the interfacial tension, analogous to softening observed in lipid bilayers. Mouritsen and coworkers [78] also applied a multi-state computer model to study fluctuations in DPPC bilayers. In these simulations domains, which fluctuated in size and position, were observed over a range of temperatures near the transition temperature. The domains increased in size as the transition temperature was approached.

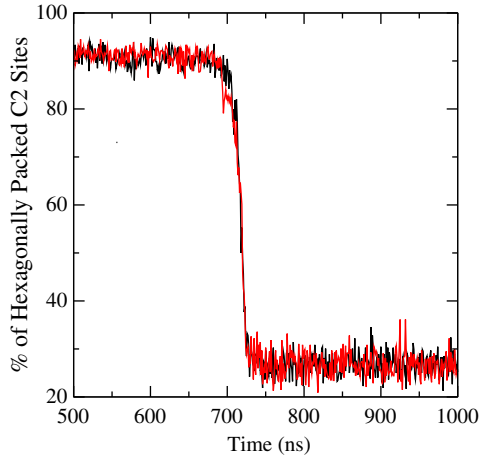

Fig. 13. Packing fluctuations. Characteristic packing fluctuations are shown here for pure DPPC monolayers heated from an initially ordered state (283K) to 323K. Both the top (red) and bottom (black) monolayers are shown. The fluctuations shown here are similar to those seen in all of our simulations, which vary slightly in magnitude. Most of our simulations that undergo a phase transition do so before 500 ns of simulation time. However, phase transitions can occur at later times as shown here.

3.9. System size effects and simulation time

As discussed previously [11,37], system-size and simulation-time artifacts should be carefully considered. This is especially true when phase transitions are involved. Simulating a biphasic system raises additional concerns about artifacts. When the box is split between phases each domain is further limited in size. Also short simulation time-scales will be associated with kinetic effects. However kinetic effects are also present in experiment (although to a lesser degree), as discussed previously [11], and physiological surfactant function is also dynamic in nature, and as such is subject to kinetic factors. While the equilibrium domain morphology is determined by the balance between line tension and long range dipole–dipole repulsion, the actual (experimental and physiological) domain morphology is normally determined by kinetic factors, since true equilibrium between phases in a monolayer is established very slowly, see [4] and references therein. Therefore, experimental phase distributions depend on compression rate, with fast compression resulting in smaller domains [4].

Hysteresis is expected to decrease with increased simulation times or larger system sizes. Previous CG-MD simulations of the gel to liquid-crystalline phase transitions in DPPC bilayers have shown that the hysteresis observed in the freezing and melting transitions depends on both system size and time-scale [46]. Previous CG-MD simulations of pressure-area isotherms of DPPC monolayers have also shown that increasing the system size decreases the hysteresis loop [11]. Here a comparison of hysteresis loops obtained from 1 μ s and 100 ns simulations of DPPC monolayers (Fig. 14) reveals a substantial change in hysteresis. As noted previously [46], the transition is triggered by a critical fluctuation, which is more likely to occur given a larger system size or a longer simulation time.

Beyond their effect on hysteresis, it is unclear what additional effects system size and simulation time may have on the evolution of the phase distribution. For instance, given long enough simulation times, domain coarsening may occur within the LC phase of the CG 1:1 DPPC:POPC monolayer, and given a larger system size SP-B_{1-25} could display a preference for the interface between the LE and LC phase. Unfortunately, the system size and time scales required to attain an equilibrium distribution of LC and LE phases are much larger than that currently accessible by molecular simulation. Although CG simulation is still limited by system size and simulation time effects, it does allow observation of dynamic phase transitions on time and length scales not yet readily accessible by atomistic simulation, whose time and distance windows are too small, or experiment, whose resolution is not small enough.

4. Summary

Using the MARTINI model, we simulated LC–LE phase transitions in monolayers containing DPPC and additional lipid or peptide components. Our analysis of DPPC monolayers suggests that the LC phase forms via a nucleation and growth mechanism analogous to that observed in lipid bilayers. In the reverse process, the melting of the LC phase is observed to originate at defects in the monolayer. Both POPC and SP-B_{1-25} are found to fluidize the monolayer. In correlation with

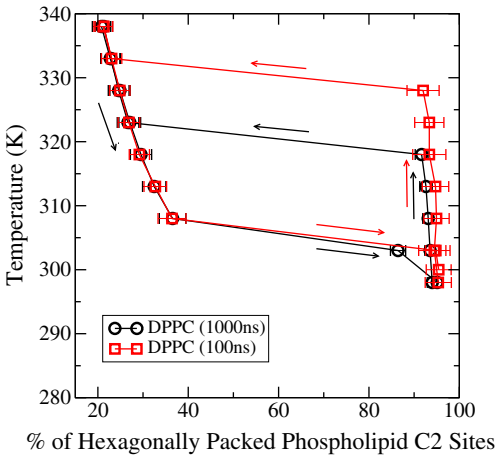

Fig. 14. Hysteresis in pure DPPC monolayers for simulations run for 1000 ns (black) and 100 ns (red) at each temperature.

experimental observations SP-B_{1-25} is found to reside in the LE phase of the monolayer. SP-B_{1-25} is also observed to perturb the packing of the surrounding lipids leading to local fluidization of the monolayer. The presence of POPC spread throughout the monolayer prohibits the DPPC condensed-phase domains from nucleating at higher temperatures. At low temperatures, both POPC and DPPC condense. The segregation of the two lipids is observed in the condensed phase, but not in the expanded phase. The DPPC–cholesterol monolayers are found to display a phase of intermediate order, which could be the liquid-disordered (Ld) phase. The hysteresis loop for DPPC–cholesterol monolayers is shifted up slightly compared to the hysteresis loop for pure DPPC, suggesting that the addition of cholesterol results in an increase in the transition temperature and stabilization of the condensed phase. Cholesterol shows a preference for the interface between the ordered and disordered lipids, in agreement with previous simulation results. DPPC displays a substantial amount of hysteresis, which is decreased by the addition of a second component. While the addition of cholesterol or POPC decreases the hysteresis loop, the addition of SP-B_{1-25} abolishes the hysteresis loop altogether. SP-B_{1-25} nucleates disorder causing the disappearance of the ordered side of the hysteresis loop. These results suggest that the presence of impurities in the monolayer (such as SP-B_{1-25}) may obviate the need for fluctuations to produce a critical nucleus for a disordering transition. These results illustrate that coarse-grained molecular dynamics simulation is a powerful tool for investigating the dynamic phase behavior of lipid and lipid–peptide monolayers on length scales not accessible by experimental methods or atomistic simulation.

References

[1] R. Veldhuizen, K. Nag, S. Orgeig, F. Possmayer, The role of lipids in pulmonary surfactant, Biochim. Biophys. Acta 1408 (1998) 90–108.
[2] Y. Zuo, R. Veldhuizen, A. Neumann, N. Petersen, F. Possmayer, Current perspectives in pulmonary surfactant: inhibition, enhancement, and evaluation, Biochim. Biophys. Acta 1778 (2008) 1947–1977.
[3] A. Günther, C. Ruppert, R. Schmidt, P. Markart, F. Grimminger, D. Walmrath, W. Seeger, Surfactant alteration and replacement in acute respiratory distress syndrome, Respir. Res. 2 (2001) 353–364.
[4] Y. Zuo, E. Keating, L. Zhao, S. Tadayyon, R. Veldhuizen, N. Petersen, F. Possmayer, Atomic force microscopy studies of functional and dysfunctional pulmonary surfactant films. I. Micro- and nanostructures of functional pulmonary surfactant films and the effect of SP-A, Biophys. J. 94 (2008) 3549–3564.
[5] R. Hite, Surfactant deficiency in adults, Clin. Pulm. Med. 9 (2002) 39–45.
[6] B. Holm, Z. Wang, E. Egan, R. Notter, Content of dipalmitoyl phosphatidylcholine in lung surfactant: ramifications for surface activity, Pediatr. Res. 39 (1996) 805–811.
[7] J. Pérez-Gil, Structure of pulmonary surfactant membranes and films: the role of proteins and lipid–protein interactions, Biochim. Biophys. Acta 1778 (2008) 1676–1695.
[8] J. Pérez-Gil, Lipid–protein interactions of hydrophobic surfactant proteins SP-B and SP-C in lung surfactant assembly and dynamics, Pediatr. Pathol. Mol. Med. 20 (2001) 445–469.
[9] T. Curstedt, J. Johansson, P. Persson, A. Eklund, B. Robertson, B. Löwenadler, H. Jörnvall, Hydrophobic surfactant-associated polypeptides: SP-C is a lipopeptide with two palmitoylated cysteine residues, whereas SP-B lacks covalently linked fatty acyl groups, Proc. Natl. Acad. Sci. U.S.A. 87 (1990) 2984–2989.
[10] T. Curstedt, H. Jörnvall, B. Robertson, T. Bergman, P. Berggren, Two hydrophobic low-molecular-mass protein fractions of pulmonary surfactant: characterization and biophysical activity, Eur. J. Biochem. 168 (1987) 255–262.
[11] S. Duncan, R. Larson, Comparing experimental and simulated pressure-area isotherms for DPPC, Biophys. J. 94 (2008) 2965–2986.
[12] G. Ma, H. Allen, DPPC Langmuir monolayer at the air–water interface: probing the tail and headgroups by vibrational sum frequency generation spectroscopy, Langmuir 22 (2006) 5341–5349.
[13] B. Piknova, W. Schief, V. Vogel, B. Discher, S. Hall, Discrepancy between phase behavior of lung surfactant phospholipids and the classical model of surfactant function, Biophys. J. 81 (2001) 2172–2180.
[14] K. Nag, S. Taneva, J. Pérez-Gil, A. Cruz, K. Keough, Combinations of fluorescently labeled pulmonary surfactant proteins SP-B and SP-C in phospholipid films, Biophys. J. 72 (1997) 2638–2650.
[15] K. Nag, J. Pérez-Gil, M. Ruano, L. Worthman, J. Stewart, C. Casals, K. Keough, Phase transitions in films of lung surfactant at the air–water interface, Biophys. J. 74 (1998) 2983–2995.
[16] C. Alonso, T. Alig, J. Yoon, F. Bringezu, H. Warriner, J. Zasadzinski, More than a monolayer: relating lung surfactant structure and mechanics to composition, Biophys. J. 87 (2004) 4188–4202.
[17] A. Cruz, L. Vázquez, M. Vélez, J. Pérez-Gil, Effect of pulmonary surfactant protein SP-B on the micro- and nanostructure of phospholipid films, Biophys. J. 86 (2004) 308–320.
[18] A. Cruz, L. Worthman, A. Serrano, C. Casals, K. Keough, J. Pérez-Gil, Microstructure and dynamic surface properties of surfactant protein SP-B/dipalmitoylphosphatidylcholine interfacial films spread from lipid–protein bilayers, Eur. Biophys. J. 29 (2000) 204–213.
[19] J. Watkins, The surface properties of pure phospholipids in relation to those of lung extracts, Biochim. Biophys. Acta 152 (1968) 293–306.
[20] J. Clements, Functions of the alveolar lining, Am. Rev. Respir. Dis. 115 (1977) 67–71.
[21] A. Bangham, C. Morley, M. Phillips, The physical properties of an effective lung surfactant, Biochim. Biophys. Acta 573 (1979) 552–556.
[22] S. Schürch, R. Qanbar, H. Bachofen, F. Possmayer, The surface-associated surfactant reservoir in the alveolar lining, Biol. Neonate 67 (Suppl 1) (1995) 61–76.
[23] A. Post, A. Nahmen, M. Schmitt, J. Ruths, H. Riegler, M. Sieber, H. Galla, Pulmonary surfactant protein C containing lipid films at the air–water interface as a model for the surface of lung alveoli, Mol. Membr. Biol. 12 (1995) 93–99.
[24] B. Piknova, V. Schram, S. Hall, Pulmonary surfactant: phase behavior and function, Curr. Opin. Struct. Biol. 12 (2002) 487–494.
[25] E. Smith, J. Crane, T. Laderas, S. Hall, Metastability of a supercompressed fluid monolayer, Biophys. J. 85 (2003) 3048–3057.
[26] W. Yan, S. Biswas, T. Laderas, S. Hall, The melting of pulmonary surfactant monolayers, J. Appl. Physiol. 102 (2007) 1739–1745.
[27] F. Lhert, W. Yan, S. Biswas, S. Hall, Effects of hydrophobic surfactant proteins on collapse of pulmonary surfactant monolayers, Biophys. J. 93 (2007) 4237–4243.
[28] A. Gopal, K. Lee, Morphology and collapse transitions in binary phospholipid monolayers, J. Phys. Chem. B 105 (2001) 10348–10354.
[29] M. Lipp, K. Lee, J. Zasadzinski, A. Waring, Phase and morphology changes in lipid monolayers induced by SP-B protein and its amino-terminal peptide, Science 273 (1996) 1196–1199.
[30] D. Takamoto, M. Lipp, A. von Nahmen, K. Lee, A. Waring, J. Zasadzinski, Interaction of lung surfactant proteins with anionic phospholipids, Biophys. J. 81 (2001) 153–169.
[31] K. Lee, Collapse mechanisms of Langmuir monolayers, Annu. Rev. Phys. Chem. 59 (2008) 771–791.
[32] J. Zasadzinski, J. Ding, H. Warriner, F. Bringezu, A. Waring, The physics and physiology of lung surfactants, Curr. Opin. Colloid Interface Sci. 6 (2001) 506–513.
[33] H. Taeusch, K.M.W. Keough, Inactivation of pulmonary surfactant and the treatment of acute lung injury, Pediatr. Pathol. Mol. Med. 20 (2001) 519–536.
[34] J. Lewis, R. Veldhuizen, The role of exogenous surfactant in the treatment of acute lung injury, Annu. Rev. Physiol. 65 (2003) 613–642.
[35] H. Taeusch, J.B. de la Serna, J. Pérez-Gil, C. Alonso, J.A. Zasadzinski, Inactivation of pulmonary surfactant due to serum-inhibited adsorption and reversal by hydrophilic polymers: experimental, Biophys. J. 89 (2005) 1769–1779.
[36] Z. Leonenko, S. Gill, S. Baoukina, L. Monticelli, J. Doehner, L. Gunasekara, F. Felderer, M. Rodenstein, L. Eng, M. Amrein, An elevated level of cholesterol impairs self-assembly of pulmonary surfactant into a functional film, Biophys. J. 93 (2007) 674–683.
[37] S. Duncan, R. Larson, Folding of lipid monolayers containing lung surfactant proteins sp-b1–25 and sp-c studied via coarse-grained molecular dynamics simulations, Biochim. Biophys. Acta 1798 (2010) 1632–1650.
[38] V. Knecht, M. Müller, M. Bonn, S. Marrink, A. Mark, Simulation studies of pore and domain formation in a phospholipid monolayer, J. Chem. Phys. 122 (2005) 24704.
[39] D. Mohammad-Aghaie, E. Macé, C. Sennoga, J. Seddon, F. Bresme, Molecular dynamics simulations of liquid condensed to liquid expanded transitions in DPPC monolayers, J. Phys. Chem. B 114 (2010) 1325–1335.
[40] S. Marrink, H. Risselada, S. Yefimov, D. Tieleman, A. de Vries, The MARTINI force field: coarse grained model for biomolecular simulations, J. Phys. Chem. B 111 (2007) 7812–7824.

[41] L. Monticelli, S. Kandasamy, X. Periole, R. Larson, D. Tieleman, S. Marrink, The MARTINI coarse-grained force field: extension to proteins, J. Chem. Theo. Comp. 4 (2008) 819–834.
[42] S. Marrink, A. de Vries, D. Tieleman, Lipids on the move: simulations of membrane pores, domains, stalks and curves, Biochim. Biophys. Acta 1788 (2009) 149–168.
[43] W. Shinoda, R. DeVane, M. Klein, Zwitterionic lipid assemblies: molecular dynamics studies of monolayers, bilayers, and vesicles using a new coarse grain force field, J. Phys. Chem. B 114 (2010) 6836–6849.
[44] J. Crane, G. Putz, S. Hall, Persistence of phase coexistence in disaturated phosphatidylcholine monolayers at high surface pressure, Biophys. J. 77 (1999) 3134–3143.
[45] S. Marrink, A. de Vries, A. Mark, Coarse grained model for semiquantitative lipid simulations, J. Phys. Chem. B 108 (2004) 750–760.
[46] S. Marrink, J. Risselada, A. Mark, Simulation of gel phase formation and melting in lipid bilayers using a coarse grained model, Chem. Phys. Lipids 135 (2005) 223–244.
[47] C. Laing, S. Baoukina, D. Tieleman, Molecular dynamics study of the effect of cholesterol on the properties of lipid monolayers at low surface tensions, Phys. Chem. Chem. Phys. 11 (2009) 1916–1922.
[48] M. Stepanova, Reversible formation of nanodomains in monolayers of dppc studied by kinetic modeling, Biophys. J. 96 (2009) 4896–4905.
[49] S. Marrink, University of Groningen. Groningen Biomolecular Sciences and Biotechnology Institute. MARTINI: biomolecular forcefield for coarse grained simulations, http://md.chem.rug.nl/marrink/coarsegrain.html, 2008.
[50] L. Gordon, K. Lee, M. Lipp, J. Zasadzinski, F. Walther, M. Sherman, A. Waring, Conformational mapping of the N-terminal segment of surfactant protein B in lipid using C-13-enhanced Fourier transform infrared spectroscopy, J. Pept. Res. 55 (2000) 330–347.
[51] J. Johansson, T. Szyperski, T. Curstedt, K. Wüthrich, The NMR structure of the pulmonary surfactant-associated polypeptide SP-C in an apolar solvent contains a valyl-rich α-helix, Biochemistry 33 (1994) 6015–6023.
[52] E. May, D. Kopelevich, A. Narang, Coarse-grained molecular dynamics simulations of phase transitions in mixed lipid systems containing LPA, DOPA, and DOPE lipids, Biophys. J. 94 (2008) 878–890.
[53] S. Marrink, A. Mark, Molecular view of hexagonal phase formation in phospholipid membranes, Biophys. J. 87 (2004) 3894–3900.
[54] S. Baoukina, S. Marrink, D. Tieleman, Lateral pressure profiles in lipid monolayers, Faraday Discuss. 144 (2010) 393–409.
[55] M. Morrow, J. Pérez-Gil, G. Simatos, C. Boland, J. Stewart, D. Absolom, V. Sarin, K. Keough, Pulmonary surfactant-associated protein SP-B has little effect on acyl chains in dipalmitoylphosphatidylcholine dispersions, Biochemistry 32 (1993) 4397–4402.
[56] A. Gericke, C. Flach, R. Mendelsohn, Structure and orientation of lung surfactant SP-C and L-α-dipalmitoylphosphatidylcholine in aqueous monolayers, Biophys. J. 73 (1997) 492–499.
[57] H. Shieh, L. Hoard, C. Nordman, The structure of cholesterol, Acta Crystallogr. B37 (1981) 1538–1543.
[58] H. Berendsen, J. Postma, W. van Gunsteren, A. Dinola, J.R. Hawk, Molecular-dynamics with coupling to an external bath, J. Chem. Phys. 81 (1984) 3684–3690.
[59] S. Baoukina, L. Monticelli, S. Marrink, D. Tieleman, Pressure-area isotherm of a lipid monolayer from molecular dynamics simulations, Langmuir 23 (2007) 12617–12623.
[60] D. van der Spoel, E. Lindahl, B. Hess, A.R. van Buuren, E. Apol, P.J. Meulenhoff, D.P. Tieleman, A.L.T.M. Sijbers, K.A. Feenstra, R. van Drunen, H.J.C. Berendsen, http://www.gromacs.org, 2005.
[61] S. Feller, Y. Zhang, R. Pastor, Computer simulation of liquid/liquid interfaces. II. Surface tension-area dependence of a bilayer and monolayer, J. Chem. Phys. 103 (1995) 10267–10276.
[62] S. Chiu, M. Clark, V. Balaji, S. Subramaniam, H. Scott, E. Jakobsson, Incorporation of surface tension into molecular dynamics simulation of an interface: a fluid phase lipid bilayer membrane, Biophys. J. 69 (1995) 1230–1245.
[63] J.L. Cascales, T. Otero, A.F. Romero, L. Camacho, Phase transition of a DPPC bilayer induced by an external surface pressure: from bilayer to monolayer behavior. A molecular dynamics study, Langmuir 22 (2006) 5818–5824.
[64] Y. Zhang, S. Feller, B. Brooks, R. Pastor, Computer simulation of liquid/liquid interfaces. I. Theory and application to octane water. J. Chem. Phys. 103 (1995) 10252–10266.
[65] S. Feller, R. Pastor, Constant surface tension simulations of lipid bilayers: the sensitivity of surface areas and compressibilities, J. Chem. Phys. 111 (1999) 1281–1287.
[66] H. Berendsen, D. van der Spoel, R. van Drunen, GROMACS — a message-passing parallel molecular-dynamics implementation, Comp. Phys. Commun. 91 (1995) 43–56.
[67] E. Lindahl, B. Hess, D. van der Spoel, GROMACS 3.0: a package for molecular simulation and trajectory analysis, J. Mol. Mod. 7 (2001) 306–317.
[68] D. van der Spoel, E. Lindahl, B. Hess, G. Groenhof, A. Mark, H. Berendsen, GROMACS: fast, flexible, and free, J. Comp. Chem. 26 (2005) 1701–1718.
[69] J. Shewchuk, Delaunay refinement algorithms for triangular mesh generation, Comput. Geom. Theory Appl. 22 (2002) 21–74.
[70] P. Davis, B. Fleming, K. Coolbear, K. Keough, Gel to liquid-crystalline transition temperature of water dispersions of two pairs of positional isomers of unsaturated mixed-acid phosphatidylcholines, Biochemistry 20 (1981) 3633–3636.
[71] J. Nagle, S. Tristram-Nagle, Structure of lipid bilayers, Biochim. Biophys. Acta 1469 (2000) 159–195.
[72] H. Hauser, I. Pascher, R. Pearson, S. Sundell, Preferred conformation and molecular packing of phosphatidylethanolamine and phosphatidylcholine, Biochim. Biophys. Acta 650 (1981) 21–51.
[73] A. Blume, M. Hillmann, Dimyristoylphosphatidic acid/cholesterol bilayers. Thermodynamic properties and kinetics of the phase transition as studied by the pressure jump relaxation technique, Eur. Biophys. J. 13 (1986) 343–353.
[74] J.B. de la Serna, J. Pérez-Gil, A. Simonsen, L. Bagatolli, Cholesterol rules, J. Biol. Chem. 279 (2004) 40715–40722.
[75] K. Tu, M. Klein, D. Tobias, Constant-pressure molecular dynamics investigation of cholesterol effects in a dipalmitoylphosphatidylcholine bilayer, Biophys. J. 75 (1998) 2147–2156.
[76] M. Patra, Lateral pressure profiles in cholesterol–dppc bilayers, Eur. Biophys. J. 35 (2005) 79–88.
[77] L. Cruzeiro-Hansson, J. Ipsen, O. Mouritsen, Intrinsic molecules in lipid membranes change the lipid-domain interfacial area: cholesterol at domain interfaces, Biochim. Biophys. Acta 979 (1989) 166–176.
[78] O. Mouritsen, Theoretical-models of phospholipid phase-transitions, Chem. Phys. Lipids 57 (1991) 179–194.
[79] S. Pandit, G. Khelashvili, E. Jakobsson, A. Grama, H. Scott, Lateral organization in lipid-cholesterol mixed bilayers, Biophys. J. 92 (2007) 440–447.
[80] H. Risselada, S. Marrink, The molecular face of lipid rafts in model membranes, Proc. Natl. Acad. Sci. U.S.A. 105 (2008) 17367–17372.
[81] R. Weis, H. McConnell, Cholesterol stabilizes the crystal liquid interface in phospholipid monolayers, J. Phys. Chem. 89 (1985) 4453–4459.
[82] E. Sparr, K. Ekelund, J. Engblom, S. Engström, H. Wennerström, An afm study of lipid monolayers. 2. Effect of cholesterol on fatty acids, Langmuir 15 (1999) 6950–6955.
[83] K. Lee, M. Lipp, J. Zasadzinski, A. Waring, Effects of lung surfactant specific protein SP-B and model SP-B peptide on lipid monolayers at the air–water interface, Colloids Surf. B Physicochem. Eng. Aspects 128 (1997) 225–242.
[84] J. Ding, D. Takamoto, A. von Nahmen, M. Lipp, K. Lee, A. Waring, J. Zasadzinski, Effects of lung surfactant proteins, SP-B and SP-C, and palmitic acid on monolayer stability, Biophys. J. 80 (2001) 2262–2272.
[85] S. Krol, M. Ross, M. Sieber, S. Kunneke, H. Galla, A. Janshoff, Formation of three-dimensional protein–lipid aggregates in monolayer films induced by surfactant protein B, Biophys. J. 79 (2000) 904–918.
[86] S. Krol, A. Janshoff, M. Ross, H. Galla, Structure and function of surfactant protein B and C in lipid monolayers: a scanning force microscopy study, Phys. Chem. Chem. Phys. 79 (2000) 904–918.
[87] M. Amrein, A. von Nahmen, M. Sieber, A scanning force- and fluorescence light microscopy study of the structure and function of a model pulmonary surfactant, Eur. Biophys. J. 26 (1997) 349–357.
[88] A. von Nahmen, M. Schenk, M. Sieber, M. Amrein, The structure of a model pulmonary surfactant as revealed by scanning force microscopy, Biophys. J. 72 (1997) 463–469.
[89] A. Kramer, A. Wintergalen, M. Sieber, H. Galla, M. Amrein, R. Guckenberger, Distribution of the surfactant-associated protein C within a lung surfactant model film investigated by near-field optical microscopy, Biophys. J. 78 (2000) 458–465.
[90] H. Galla, N. Bourdos, A. von Nahmen, M. Amrein, M. Sieber, The role of pulmonary surfactant protein C during the breathing cycle, Thin Solid Films 327–329 (1998) 632–635.
[91] R. Sibug-Aga, R. Dunn, High-resolution studies of lung surfactant collapse, Photochem. Photobiol. 80 (2004) 471–476.
[92] M. Lipp, K. Lee, D. Takamoto, J. Zasadzinski, A. Waring, Coexistence of buckled and flat monolayers, Phys. Rev. Lett. 81 (1998) 1650–1653.
[93] P. Nakorn, M. Meyer, C. Flach, R. Mendelsohn, H. Galla, Surfactant protein C and lung function: new insights into the role of α-helical length and palmitoylation, Eur. Biophys. J. 36 (2007) 477–489.
[94] L. Wang, P. Cai, H. Galla, H. He, C. Flach, R. Mendelsohn, Monolayer-multilayer transitions in a lung surfactant model: IR reflection–absorption spectroscopy and atomic force microscopy, Eur. Biophys. J. 34 (2005) 243–254.
[95] R. Diemel, M. Snel, A. Waring, F. Walther, L. van Golde, G. Putz, H. Haagsman, J. Batenburg, Multilayer formation upon compression of surfactant monolayers depends on protein concentration as well as lipid composition. An atomic force microscopy study, J. Biol. Chem. 277 (2002) 21179–21188.
[96] J. Ding, I. Doudevski, H. Warriner, T. Alig, J. Zasadzinski, Nanostructure changes in lung surfactant monolayers induced by interactions between palmitoyloleoylphosphatidylglycerol and surfactant protein B, Langmuir 19 (2003) 1539–1550.
[97] N. Bourdos, F. Kollmer, A. Benninghoven, M. Ross, M. Sieber, H. Galla, Analysis of lung surfactant model systems with time-of-flight secondary ion mass spectrometry, Biophys. J. 79 (2000) 357–369.
[98] W. Schief, M. Antia, B. Discher, S. Hall, V. Vogel, Liquid-crystalline collapse of pulmonary surfactant monolayers, Biophys. J. 84 (2003) 3792–3806.
[99] S. Malcharek, A. Hinz, L. Hilterhaus, H. Galla, Multilayer structures in lipid monolayer films containing surfactant protein c: effects of cholesterol and pope, Biophys. J. 88 (2005) 2638–2649.
[100] O. Mouritsen, J. Ipsen, M. Zuckermann, Lateral density fluctuations in the chain-melting phase transition of lipid monolayers, J. Colloid Interface Sci. 129 (1988) 32–40.